N62-16296

TECHNICAL NOTE

D-1381

LOW-SPEED STATIC LONGITUDINAL AND LATERAL AERODYNAMIC

CHARACTERISTICS OF A MODEL WITH A LOW-ASPECT-RATIO

VARIABLE-INCIDENCE WING AND WITH A FREE-FLOATING

AND A PROGRAMED HIGH-LIFT CANARD CONTROL

By William I. Scallion

Langley Research Center
Langley Station, Hampton, Va.

OTS PRICE

XEROX

MICROFILM

NATIONAL AERONAUTICS AND SPACE ADMINISTRATION

WASHINGTON   October 1962

NATIONAL AERONAUTICS AND SPACE ADMINISTRATION

TECHNICAL NOTE D-1381

LOW-SPEED STATIC LONGITUDINAL AND LATERAL AERODYNAMIC CHARACTERISTICS OF A MODEL WITH A LOW-ASPECT-RATIO VARIABLE-INCIDENCE WING AND WITH A FREE-FLOATING AND A PROGRAMED HIGH-LIFT CANARD CONTROL

By William I. Scallion

SUMMARY

An investigation was conducted in the Langley full-scale tunnel to determine the static longitudinal and lateral aerodynamic characteristics of two low-aspect-ratio variable-incidence delta-wing models equipped with canard controls. One model was tested with a free-floating canard and with twin vertical tails mounted on the wing tips, and the other model was tested with a programed high-lift canard and with a single vertical tail mounted on the body center line.

The results indicated that at moderate to high trim lift coefficients the configuration with the programed high-lift canard had a wider center-of-gravity range for longitudinal stability than either a fixed- or free-floating-canard configuration. At a given angle of attack, the free-floating-canard configuration with a variable-incidence wing had a greater center-of-gravity range for longitudinal stability than a comparable configuration having a fixed wing with trailing-edge flaps. The results also showed that the flow field of the programed high-lift canard adversely affected the lift, longitudinal stability, and effective dihedral characteristics of the model.

INTRODUCTION

The low-speed performance of canard airplanes is limited in general by the longitudinal trim effectiveness of the canard surface. Previous investigations have shown that the performance of canard configurations having low wing aspect ratios can be improved by free-floating the canard control (ref. 1) or by increasing the lifting capability of the canard control with high-lift devices (ref. 2). Reference 2 also showed that the wing lift could be increased more at a given angle of attack with less diving moment by varying wing incidence than by use of a wing flap.

A study of the results of the two investigations indicated that combinations of some of the features of the reference test models would prove advantageous in providing high trim lift coefficients. Accordingly, an investigation of the low-speed characteristics of two canard configurations that utilized combinations of the features of the models of references 1 and 2 was conducted in the Langley full-scale tunnel. The first configuration consisted of the variable-incidence delta-wing model of reference 2 equipped with a free-floating canard. It was expected that the use of the variable-incidence wing with the free-floating canard would result in a higher trim lift coefficient at a given angle of attack than that obtained with the flapped configuration of reference 1. The second configuration consisted of the same model equipped with a high-lift canard programed to simulate a floating canard surface driven by an angle-of-attack sensor. This configuration would combine the high-lift characteristics of the fixed-canard configuration and the longitudinal stability characteristics of the free-floating-canard configuration.

The purpose of the tests was to determine the static longitudinal and lateral aerodynamic characteristics and the longitudinal control effectiveness of the two canard configurations. The effectiveness of wing flaps, wing incidence, and combinations of flap and incidence as high-lift devices was also studied.

COEFFICIENTS AND SYMBOLS

The longitudinal aerodynamic data are referred to the stability system of axes and the lateral data are referred to the body system of axes as shown in figure 1. The coefficients and symbols used are defined as follows:

C_D drag coefficient, $\dfrac{\text{Drag}}{q_\infty S}$

C_L lift coefficient, $\dfrac{\text{Lift}}{q_\infty S}$

$C_{L,\text{trim}}$ trim lift coefficient

C_l rolling-moment coefficient, $\dfrac{\text{Rolling moment}}{q_\infty S b}$

C_m pitching-moment coefficient, $\dfrac{\text{Pitching moment}}{q_\infty S \bar{c}}$

C_n yawing-moment coefficient, $\dfrac{\text{Yawing moment}}{q_\infty Sb}$

C_Y side-force coefficient, $\dfrac{\text{Side force}}{q_\infty S}$

$C_{\mu,t}$ canard-surface momentum coefficient, $\dfrac{GV_j}{q_\infty S_t}$

$\dfrac{dC_m}{dC_L}$ rate of change of pitching-moment coefficient with respect to lift coefficient

$\dfrac{di_t}{d\alpha}$ rate of change of canard-surface incidence with model angle of attack

C_{l_β} $\dfrac{\partial C_l}{\partial \beta}$ (slopes measured from $\beta = -5^\circ$ to 5° or $\beta = 0^\circ$ to 5°), per degree

C_{n_β} $\dfrac{\partial C_n}{\partial \beta}$ (slopes measured from $\beta = -5^\circ$ to 5° or $\beta = 0^\circ$ to 5°), per degree

C_{Y_β} $\dfrac{\partial C_Y}{\partial \beta}$ (slopes measured from $\beta = -5^\circ$ to 5° or $\beta = 0^\circ$ to 5°), per degree

b wing span, ft

$\bar{c}$ wing mean aerodynamic chord, ft

G mass rate of airflow, slugs/sec

q_∞ free-stream dynamic pressure, lb/sq ft

S wing area, sq ft

S_t canard-surface total area, sq ft

V_j velocity of blowing jet, ft/sec

x longitudinal distance from leading edge of wing mean aerodynamic chord to center of gravity, positive rearward, ft

α angle of attack of model reference line, deg

α_{trim} angle of attack of model, longitudinally trimmed

α_t canard-surface nominal angle of attack (i_t measured at $\alpha = 0^\circ$), deg

i_t canard-surface incidence, relative to model reference line, deg

i_w wing incidence, relative to model reference line, deg

δ_f wing-flap deflection angle with respect to wing chord line, deg

$\delta_{f,t}$ canard-surface-flap deflection angle with respect to canard-surface chord line, deg

β angle of sideslip, deg

MODELS

The general arrangement and principal dimensions of the models are presented in figures 2 and 3, and detailed geometric data on the models and components are given in table I. Both models utilized the basic delta-wing body described in reference 2. The wing had a truncated delta planform of aspect ratio 1.47, with a 60° swept leading edge, and NACA 65A003 airfoil sections parallel to the plane of symmetry. The wing was pivoted about an axis through the 53-percent station of the mean aerodynamic chord to allow variation of wing incidence relative to the fuselage reference line.

Model I

Model I, which is shown in figure 2, was equipped with a free-floating canard having a delta planform. The canard was free to pivot about the midpoint of the projected root chord line, and this hinge line was located $1.45\bar{c}$ ahead of the model balance center ($0.275\bar{c}$ point on the wing). The canard was statically balanced about the hinge line, and canard deflection was obtained by attaching preset tabs to the trailing edges. (See fig. 2.) Twin outboard vertical tails were mounted on the wing tips and were located such that 33.4 percent of the tail area was below the wing chord plane.

Model II

The general arrangement and principal dimensions of model II are shown in figure 3. A photograph of the model is shown in figure 4. The low-aspect-ratio trapezoidal canard used with the model was the same

as the one described and designated canard A in reference 2. It was equipped with a leading-edge slat and a full-span trailing-edge-blowing flap for high lift effectiveness. In addition to the original canard location of 7.75 inches below the wing pivot plane, the canard could be located on the wing pivot plane by installing a metal bracket on top of the body. As shown in figure 3, the model had a single fuselage-mounted vertical tail and twin outboard ventral fins mounted on the underside of the wing. The wing was equipped with constant-chord plain flaps having a total span of 53.5 percent of the wing span.

TESTS

The tests were conducted in the Langley full-scale tunnel at angles of attack ranging from -4° to 24° except for one case where the range was extended to 28°. Both models were tested with wing incidence angles of 0°, 8°, and 12° at sideslip angles of -10°, -5°, 0°, 5°, and 10°. Force and moment measurements were made with a six-component internal strain-gage balance. The test Reynolds number based on the mean aerodynamic chord was 2.4×10^6 and the Mach number was 0.10. The calculated jet boundary and buoyancy effects were negligibly small and therefore were not applied to the data.

Model I

Model I was tested with the canard free-floating without tabs and with tabs attached to provide canard deflections for trim. The canard deflections relative to the model reference line were visually recorded by reading a quadrant painted on the model nose. The canard angles of incidence i_t at zero model angle of attack were 0° or 1° without trailing-edge tabs and were 16°, and 24° or 25°, with the two trailing-edge tabs. These angles are used in the remainder of the paper as the nominal angles of attack of the canard α_t.

Model II

The tests were conducted on model II with a programed high-lift canard for wing incidence angles of 0° and 8° with the wing flaps deflected 30° and for $i_w = 12^\circ$ with the flaps deflected 10°, 20°, and 30°. The canard was remotely driven and was programed to simulate the constant-angle-of-attack characteristics of a free-floating canard. The variation of canard incidence with angle of attack $di_t/d\alpha$ was found from the tests of model I with the delta planform canard to be -1.25. With use of this programing, the canard effectiveness was obtained for

values of α_t of -5°, 0°, 5°, 10°, 15°, and 20°, with and without blowing on the canard flaps. Most of the tests were conducted with the canard located 7.75 inches below the wing pivot plane, but some additional tests were made with the canard located on the wing pivot plane as shown in figure 3.

In addition to the force tests, the flow field of the canard was obtained in a plane (shown in fig. 3) 62 inches behind the nose of the model at a model angle of attack of 8°. The wing was removed for these tests.

RESULTS AND DISCUSSION

Longitudinal Characteristics

Model I.- The results of the static longitudinal tests of model I are presented for i_w = 0°, 8°, and 12° in figures 5, 6, and 7, respectively. The small plots in the upper left-hand corner of figures 5(a), 6(a), and 7(a) show the variation of i_t with α for three canard angles of attack α_t. This variation was essentially linear and was found to have an average value of -1.25. In general, the free-floating canard provided longitudinal trim to the highest model angle of attack tested at i_w = 0°, 8°, and 12°; however, the longitudinal stability was nearly neutral for the center-of-gravity location of $0.275\bar{c}$. Actually the canard could trim the model to the maximum angle of attack with center-of-gravity locations shifted forward for some degree of longitudinal stability.

Model II.- The static longitudinal characteristics of model II are presented in figures 8 to 18. Examination of the data in parts (a) of figures 8 to 17 indicates that longitudinal trim could be obtained for all combinations of wing incidence and flap deflections tested. In addition, one of the more obvious results was a break in lift-curve slope accompanied by abrupt variations in pitching-moment coefficient with lift coefficient in the form of a pitch-up that occurred between values of C_L of 0.8 and 1.0 as shown in figures 10 to 16. This pitch-up was apparently caused by the interference effects of the downwash from the highly loaded canard on the wing; and the degree to which the wing lift and moment characteristics were affected depended upon the strength of the canard downwash, the loading on the wing, and the position of the wing in the downwash field. Of the three factors mentioned, the position of the wing in the canard downwash field was the only one that could be varied without adversely affecting the longitudinal trim performance. In order to obtain the effects of wing position in the canard downwash, the canard was moved up to the wing

pivot plane and the results are presented in figure 17. The conditions for which these results were obtained were $i_w = 12^\circ$, $\delta_f = 10^\circ$, and $C_{\mu,t} = 0.025$, and they are directly comparable to the results shown in figure 12. For the identical conditions of $\alpha_t = 10^\circ$ in figures 12(a) and 17(a), it is apparent that the higher canard position resulted in the elimination of the pitch-up between $C_L = 0.8$ and 1.0, but an unstable break in the curves for $\alpha_t = 5^\circ$ and 10° exists at a lift coefficient of about 1.2. Figure 18 shows the relative location of the wing (at $i_w = 12^\circ$) in the canard downwash field with the canard in the low and high positions. The conditions shown in this figure duplicate those for the force-test results for $\alpha_t = 10^\circ$ shown in figures 12(a) and 17(a) where the force tests showed that the pitch-up and loss in lift occurred for the low canard location (see fig. 12(a)), but did not occur for the high canard location (see fig. 17(a)). As can be seen in figure 18(a) the wing is immersed in the canard flow field with the canard in the low position. From this figure it may be reasoned that the nose-up pitching moments were caused by flow separation on the out-board section of the wing resulting from the increased upwash in that region. It may further be reasoned that the reduction in lift for this condition was caused by a combination of the stalled outboard portion of the wing and the downwash over the inboard portion of the wing. Figure 18(b) shows that the wing is outside of the major portion of the canard flow field with the canard in the high position and this explains the improved results shown in figure 17(a).

Lateral Characteristics

The static lateral characteristics are presented in figures 19 to 28 in the form of plots of C_{Y_β}, C_{n_β}, and C_{l_β} against C_L.

Model I.- The static lateral characteristics of model I for $i_w = 0^\circ$, 8°, and 12° are shown in figures 19, 20, and 21, respectively. These results show that the model was generally directionally stable for lift coefficients up to about 1.0. Deflection of the canard surface for trim increased the directional stability at lift coefficients above 0.5 to 0.7 and produced an opposite trend below these coefficients for all three wing incidence angles tested. A comparison of the curves for the canard on with those for the canard off shows that the aforementioned effects may be attributed to wake effects of the canard, when highly loaded, on the wing and vertical tails. The model exhibited positive effective dihedral $\left(-C_{l_\beta}\right)$ through the lift-coefficient range tested.

In general, there were no large variations in C_{l_β} with lift coefficient.

Model II.- The static lateral characteristics of model II are shown in figures 22 to 28. Figures 25 to 28 generally show that the high-lift configuration ($i_w = 12°$) was directionally stable to lift coefficients approaching the maximum. The most noticeable result shown by these figures is the large values of C_{l_β} which were generally of the order of -0.008. The peak values of C_{l_β} occurred between lift coefficients of 0.8 to 1.0, where the losses in lift and longitudinal instability previously discussed occurred. It appears that C_{l_β} was influenced by the same factors that affected the lift and longitudinal stability of the model, namely, the interference effects of the canard downwash on the wing. In this case, the increased values of C_{l_β} were caused by the asymmetrical distribution of the canard downwash on the wing when the model was at an angle of sideslip. The canard downwash was predominantly shifted to the trailing wing during sideslip and, consequently, large rolling moments resulted.

Figure 26 shows that when the canard was moved to the wing pivot plane the variation of C_{l_β} with C_L was smoother and no abrupt peak values occurred; however, the values of C_{l_β} were high throughout the lift-coefficient range, the maximum value being about -0.008.

Because of the high values of C_{l_β} incurred by the model, it appears that sideslip angles greater than 5° or 6° could produce rolling moments beyond the limits of conventional controls such as ailerons or spoilers.

Analysis of Data

The longitudinal and lateral data are summarized in figures 29 to 32 in the form of plots of trim lift coefficient against center-of-gravity location in fractions of the mean aerodynamic chord. These curves define the highest trim lift coefficient attainable for a given center-of-gravity location. Superimposed on these plots are boundaries of longitudinal stability $\left(dC_m/dC_L = 0 \right)$. The longitudinal stability boundaries were derived from the basic longitudinal data of figures 5 to 17. Where the curves of C_m plotted against C_L did not show abrupt changes in longitudinal stability, the corresponding stability boundaries were plotted in the summary figures as straight lines representing the center-of-gravity location at which the longitudinal stability became zero. This type of boundary is shown in figures 29 to 31(a). In figures 31(b), (c), and (d), the longitudinal stability boundaries more nearly represent the actual trends in zero longitudinal stability shown in the basic data of figures 11(a), 12(a), and 13(a). Additionally, dashed lines representing zero directional

stability are plotted in these figures, but the general discussion that follows covers only the longitudinal characteristics of the model. Although these curves were obtained for a specific vertical-tail configuration for each model, and cannot be construed as general in nature, they serve to illustrate the effects of center-of-gravity location on directional stability. The average angle of attack for a given trim lift coefficient is shown on the right-hand scale in each figure.

Model I.- The static aerodynamic characteristics of model I are summarized in figure 29 for $i_w = 0^O$, 8°, and 12°. A comparison of the stability boundaries and trim lift curves shows that both the boundaries and trim lift curves are about the same for all three wing incidence angles. This indicates that for a given center-of-gravity location and lift coefficient there would be only a small change in longitudinal stability and trim requirements with a change in wing incidence. A wing incidence of 12° would result in a reduction in fuselage attitude of about 10° for a landing lift coefficient of 1.10.

Figure 30 shows a comparison of the longitudinal trim characteristics of model I with $i_w = 12^O$ and the model of reference 1 with full-span wing flaps deflected 20°. (See fig. 20, ref. 1.) As can be seen from figure 30, the trim lift coefficients for a given angle of attack are about equal at angles of attack of 12° to 16°. Within this angle-of-attack range, model I has about two to four times the center-of-gravity range for longitudinal stability as that of the flapped configuration of reference 1, although the configuration of reference 1 had a much larger canard than model I of the present investigation (20-percent wing area compared to 15-percent wing area). This comparison shows that, at least in the longitudinal sense, low-aspect-ratio wing-canard configurations can obtain a greater center-of-gravity range by utilizing wing incidence rather than flaps for additional lift at low speeds. Figure 30 also shows that the flapped configuration of reference 1 had a higher maximum trim lift coefficient, but because of the high angle of attack required, the attainment of this lift coefficient near the ground might be considered impractical.

Model II.- The static aerodynamic characteristics of model II are summarized in figure 31. As can be seen in figures 31(b) to 31(d), both the rearward and forward center-of-gravity locations were limited by longitudinal instability. The forward center-of-gravity locations were limited by longitudinal instability produced by the effects of the canard downwash on the wing, rather than the trim effectiveness of the canard. This result is shown by the small islands of longitudinal instability in figures 31(b), (c), and (d). Of the three high-lift configurations shown in these figures, the configuration with the wing flaps deflected 10° and with blowing on the canard flap (fig. 31(c)) had the widest range of center-of-gravity locations for which longitudinal stability existed.

Comparison of model I, model II, and fixed-canard configuration.-
A comparison of the longitudinal trim characteristics of model I, model II, and a fixed-canard configuration of reference 2 is shown in figure 32. The data from reference 2 are for a configuration identical to model II of the present investigation, except that the data of reference 2 were obtained with the canard fixed. The curves for models I and II (with appropriate longitudinal stability boundaries) were taken from figures 29(c) and 31(c), respectively. The comparison is not entirely valid, in that the free-floating canard of model I had a planform different from that of the other two, and the vertical-tail arrangement was also different; however, all three are compared on the basis of the optimum configurations derived from the separate test results.

The curves in figure 32 show that the same wing-body configuration requires a different center-of-gravity range for longitudinal stability for each of the canard-control systems used for longitudinal trim. The fixed-canard configuration required center-of-gravity locations ahead of $x/\bar{c} = 0.05$ whereas the free-floating canard of model I had a rearward center-of-gravity limit of $0.23\bar{c}$. The available trim lift coefficient limited the forward center-of-gravity location of all three models. It might be expected that the center-of-gravity range for longitudinal trim of the programed high-lift canard of model II should completely overlap those of model I and the configuration of reference 2; however, the canard interference effects on the longitudinal stability of the model limited the rearward center-of-gravity location. The reduced $C_{L,trim}$ for forward center-of-gravity locations resulted from the increased trim requirements imposed by the wing-flap deflection of 10° on model II. Although the configuration with the programed high-lift canard did not have as wide a center-of-gravity range for longitudinal stability as might be expected, the results do indicate that it is considerably larger than that of either the fixed-canard or free-floating-canard configurations at moderate to high trim lift coefficients.

Additional aspects of the programed high-lift canard.- Several additional characteristics of the programed high-lift canard are apparent. One, the trim input of the canard can be mechanically limited to angles less than the stall angle of attack of the canard (a characteristic in common with the free-floating canard); thus, canard stall can be avoided. Two, the ratio of sensor output for canard floating angle to input to the sensor can be varied to produce a variation in the static longitudinal stability of the model. An illustration of this idea is shown in figure 33, in which pitching-moment data of figure 14(a) have been replotted to show the effect of increasing the rate of canard incidence with angle of attack $di_t/d\alpha$ for a center-of-gravity location of $0.275\bar{c}$. The data of figure 15 are repeated in figure 33(a). The data representing increases in $di_t/d\alpha$ to 1.2 and 1.4 are shown in figures 33(b) and 33(c), respectively. It can be noted that there is an overall

increase in the static longitudinal stability with an increase in
$di_t/d\alpha$; however, the nonlinearities in the curves are accentuated in
some cases.

The curves of figure 33 show that static longitudinal stability of
an airplane with a programed high-lift canard can be increased arti-
ficially without moving the center of gravity forward. The relative
effects of this artificial method on the damping in pitch and the dynamic
stability characteristics of such an arrangement are considered to be
beyond the scope of this paper.

Another topic worth mentioning is the effect of a failure of the
sensor output to the canard. This would result in a longitudinally
unstable configuration since the center-of-gravity location would nor-
mally be rearward of that required for stability with the canard fixed;
therefore, longitudinal control would be difficult to maintain.

A failure of the pilot-generated control input would result in a
longitudinally stable, but uncontrollable, configuration. A failure of
the canard pivot, such as one that would render the canard immobile,
would result in a loss of control and a longitudinally unstable
configuration.

SUMMARY OF RESULTS

The results of the investigation of the low-speed static longitudinal
and lateral aerodynamic characteristics of a model with a low-aspect-ratio
variable-incidence wing equipped with a free-floating and a programed
high-lift canard may be summarized as follows:

1. At moderate to high trim lift coefficients the programed high-
lift canard configuration had a wider center-of-gravity range for lon-
gitudinal stability than either a fixed- or free-floating-canard
configuration.

2. The center-of-gravity range for longitudinal stability for a
free-floating-canard configuration having a low-aspect-ratio wing is
larger at a given angle of attack when wing incidence, rather than
trailing-ed flaps, is utilized for increased lift.

3. Wit the canard located below the wing pivot point, the flow
field of t..e programed high-lift canard had detrimental effects on
the lift, longitudinal stability, and lateral stability character-
istics of the model. Moving the canard up to the plane of the

wing pivot point reduced the effect of the canard flow field on the longitudinal characteristics, but the detrimental lateral characteristics produced by the canard were still present.

Langley Research Center,
National Aeronautics and Space Administration,
Langley Station, Hampton, Va., May 24, 1962.

REFERENCES

1. Scallion, William I., and Cannon, Michael D.: The Low-Speed Static Longitudinal and Lateral Characteristics of a Delta-Wing Model With Fixed and Free-Floating Canard Surfaces. NASA TM X-120, 1959.

2. Cone, Clarence D., Jr.: Low-Speed Static Longitudinal and Lateral Stability Characteristics of a Variable-Incidence Delta-Wing Canard Model With High-Lift Canard Surfaces. NASA TM X-72, 1959.

TABLE I

MODEL GEOMETRIC DATA

Wing:
Area, total projected, sq ft	14.831
Area, movable, sq ft	13.164
Span, ft	4.667
Mean aerodynamic chord, ft	3.583
Aspect ratio	1.47
Leading-edge sweep, deg	60
Airfoil section	NACA 65A003

	Model I	Model II
Canard surfaces:		
Planform	Delta	Trapezoidal
S_t/S	0.15	0.15
Aspect ratio	2.31	3.00
Taper ratio	0	0.41
Vertical tails:		
Area, total, sq ft	2.962	3.160
Aspect ratio	1.05	0.97

Ventral fins (each), model II only:
Area, sq ft	0.757
Length, ft	2.166
Maximum width, ft	0.417

Fuselage:
Length, ft	10.833
Maximum diameter, ft	1.000
Fineness ratio	10.833

14
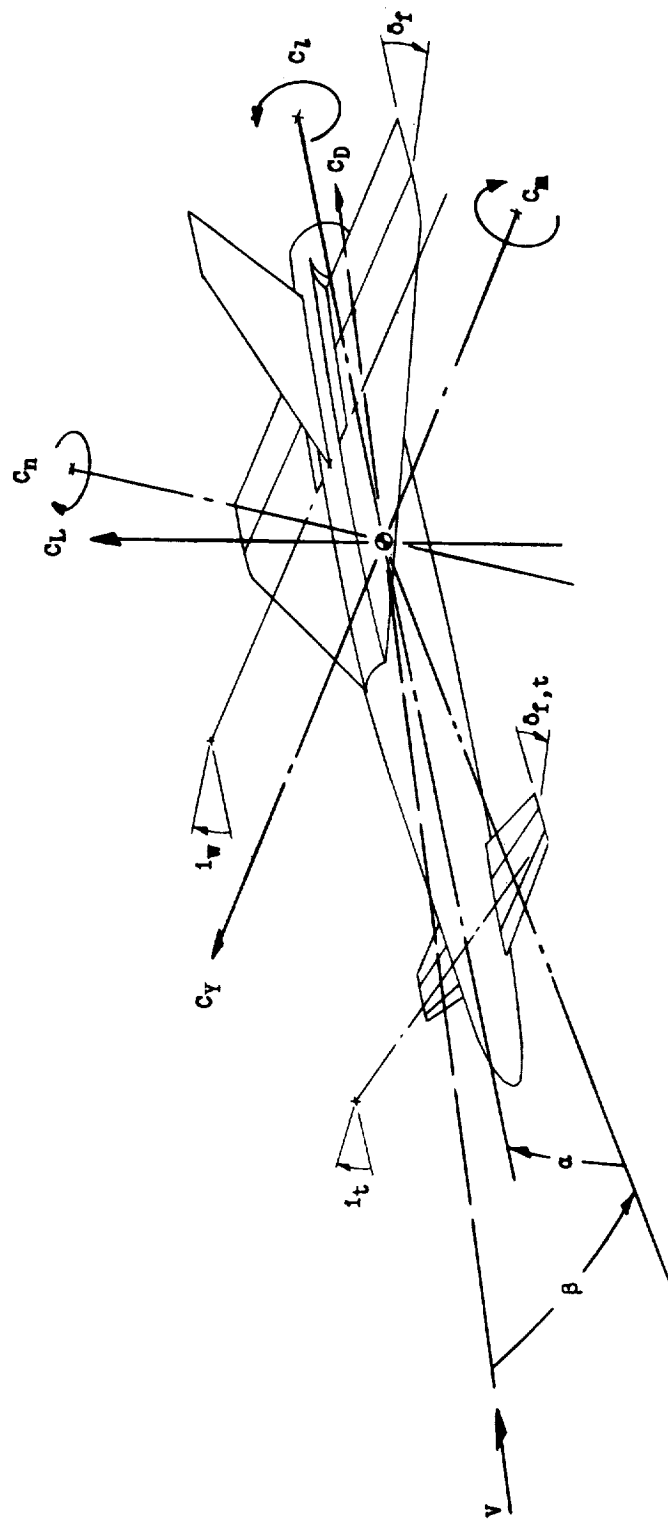
Figure 1.- System of axes used. Arrows indicate positive directions of force and moment coefficients and angular displacements.
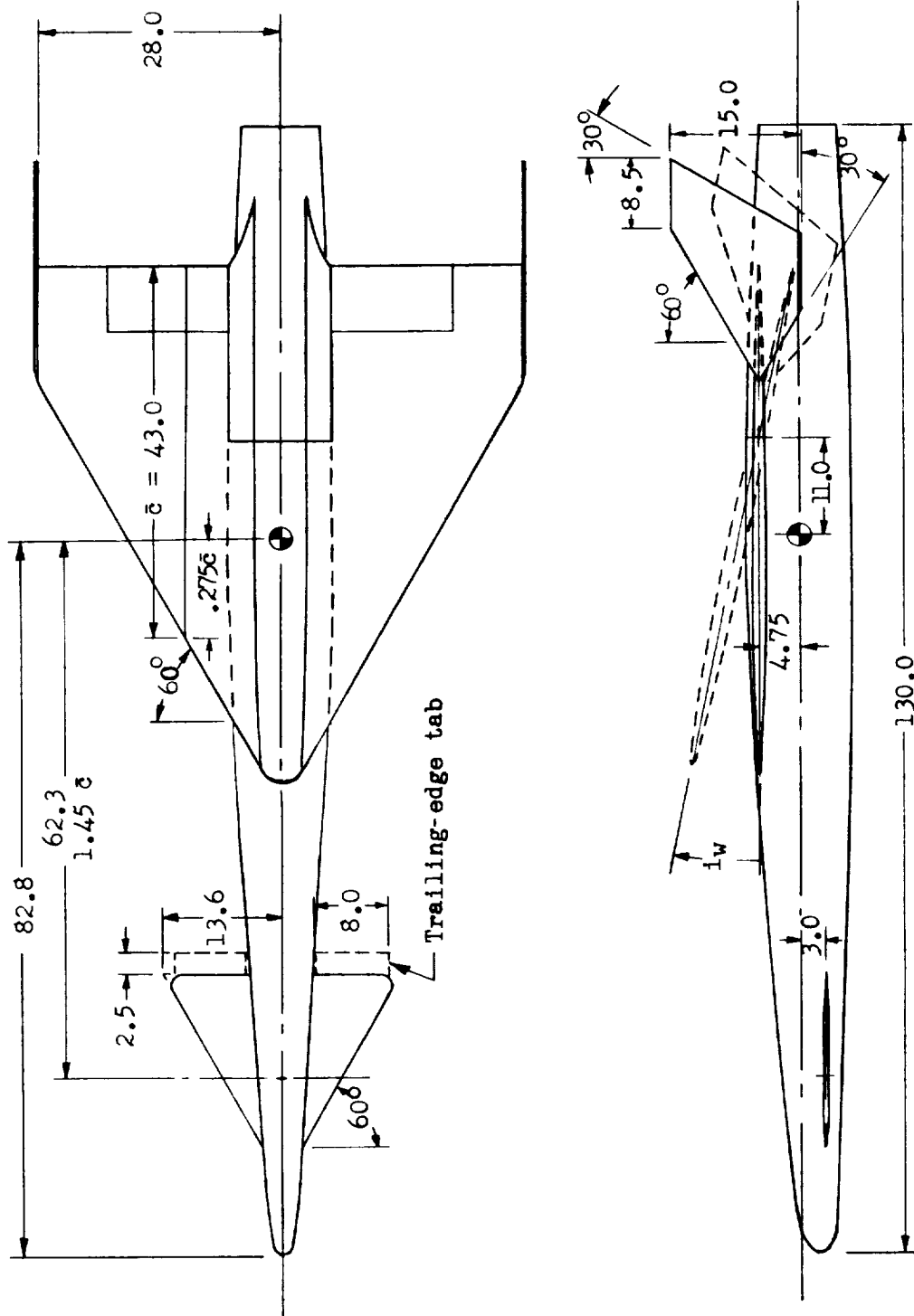
Figure 2.- Principal dimensions of model I. All dimensions are in inches.
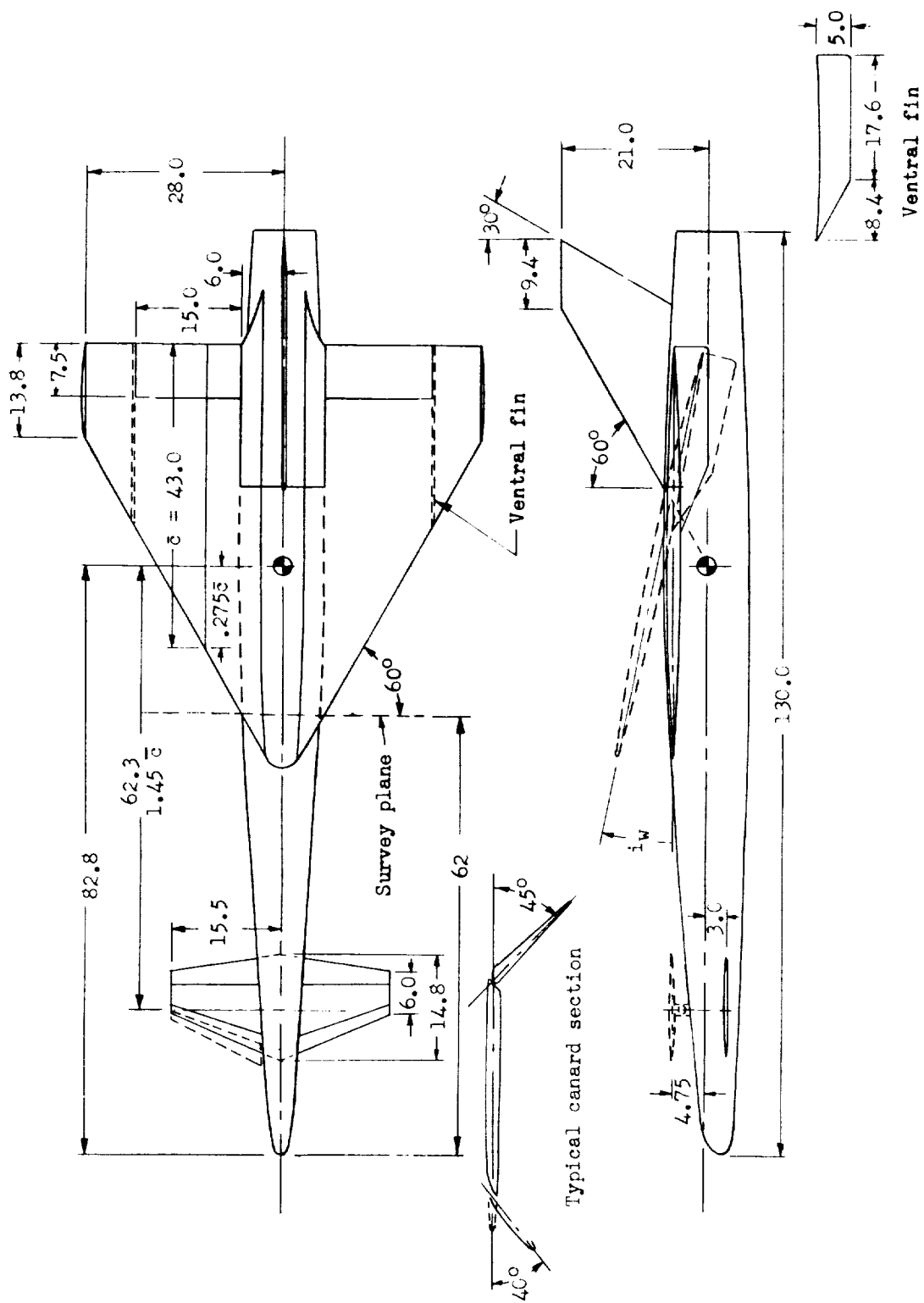
Figure 3.- Principal dimensions of model II. All dimensions are in inches.

18
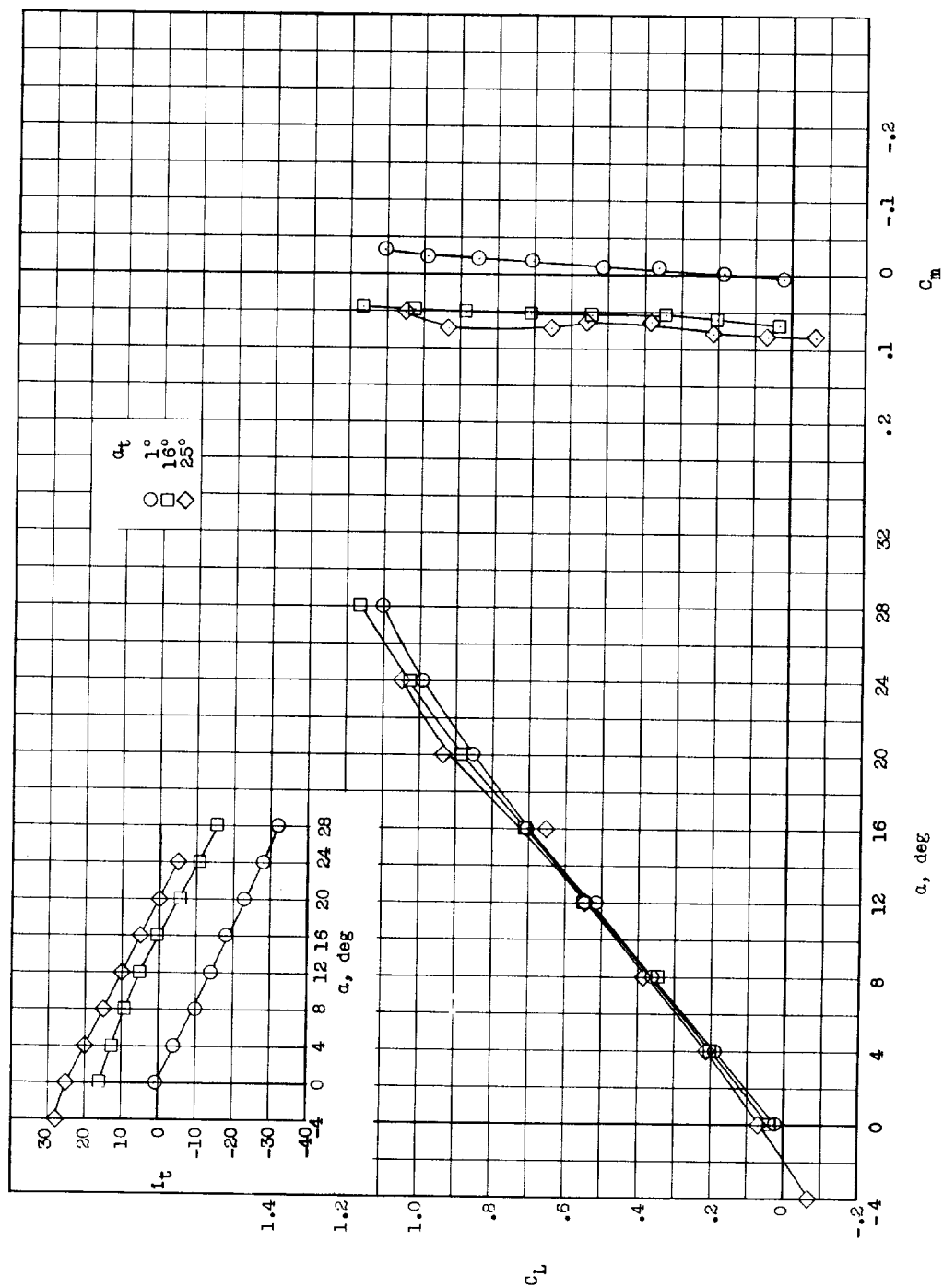
(a) Lift and pitching moment.

Figure 5.- Longitudinal characteristics of model I. $i_W = 0°$; center of gravity located at $0.275\bar{c}$.
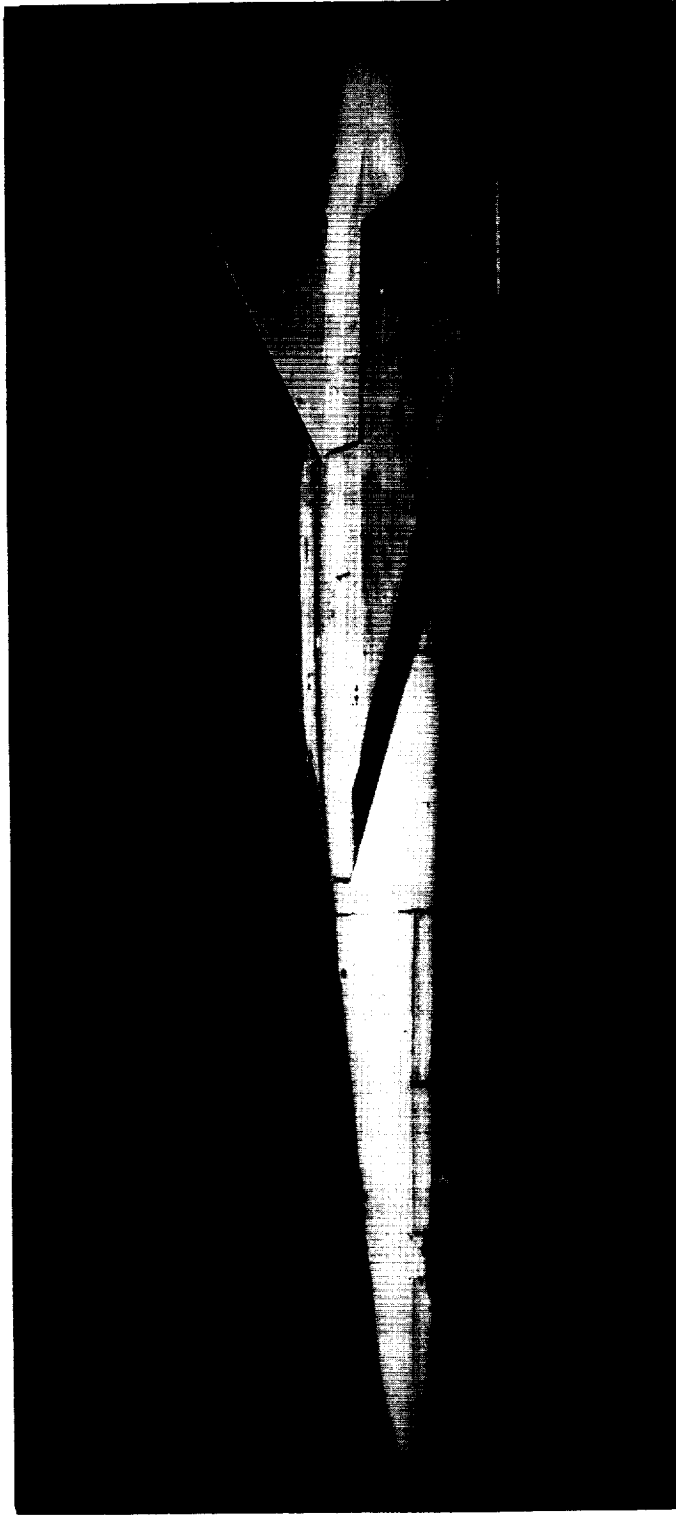
L-59-3694

Figure 4.- Photograph of model II.
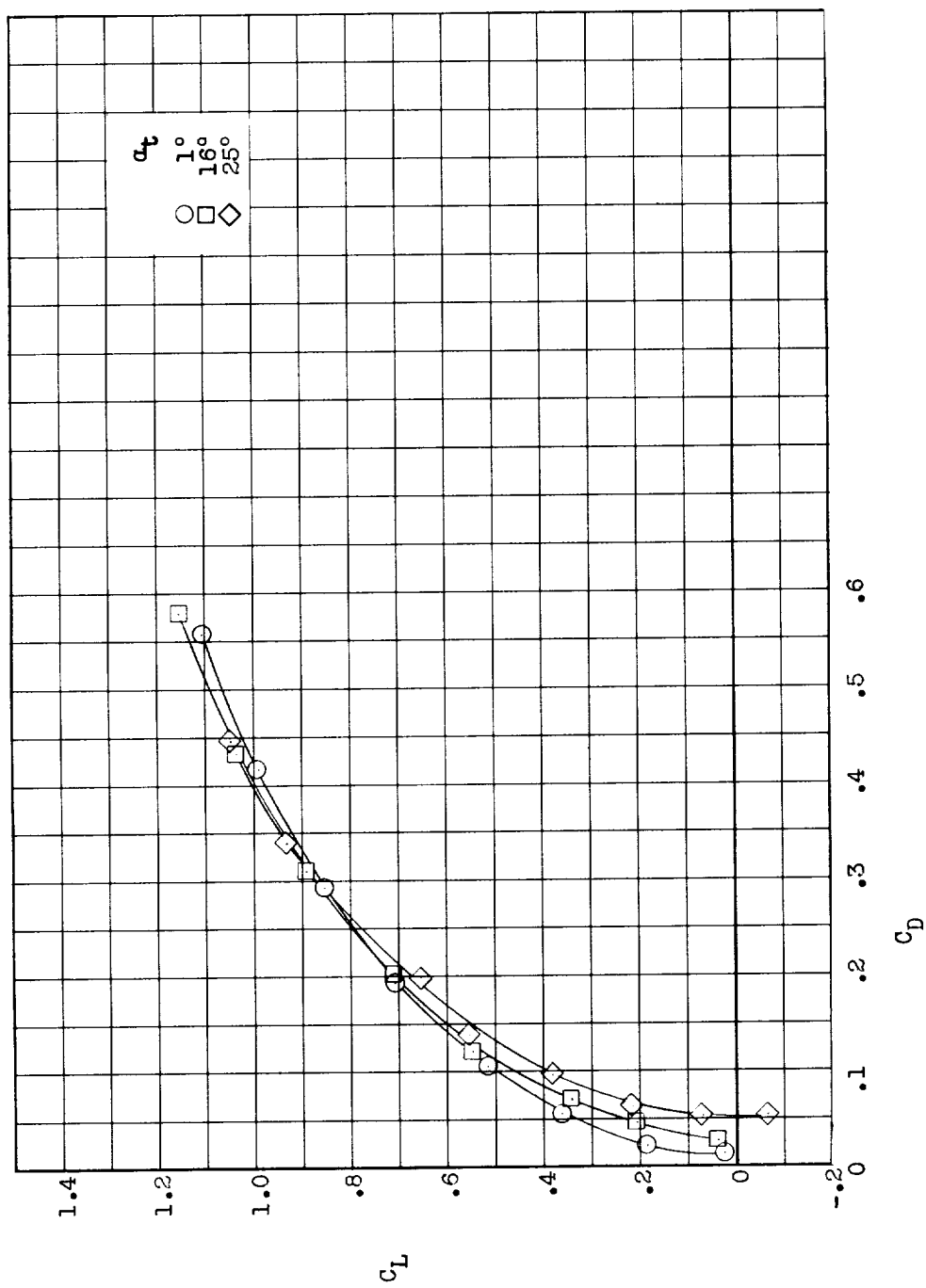
(b) Drag.

Figure 5.- Concluded.
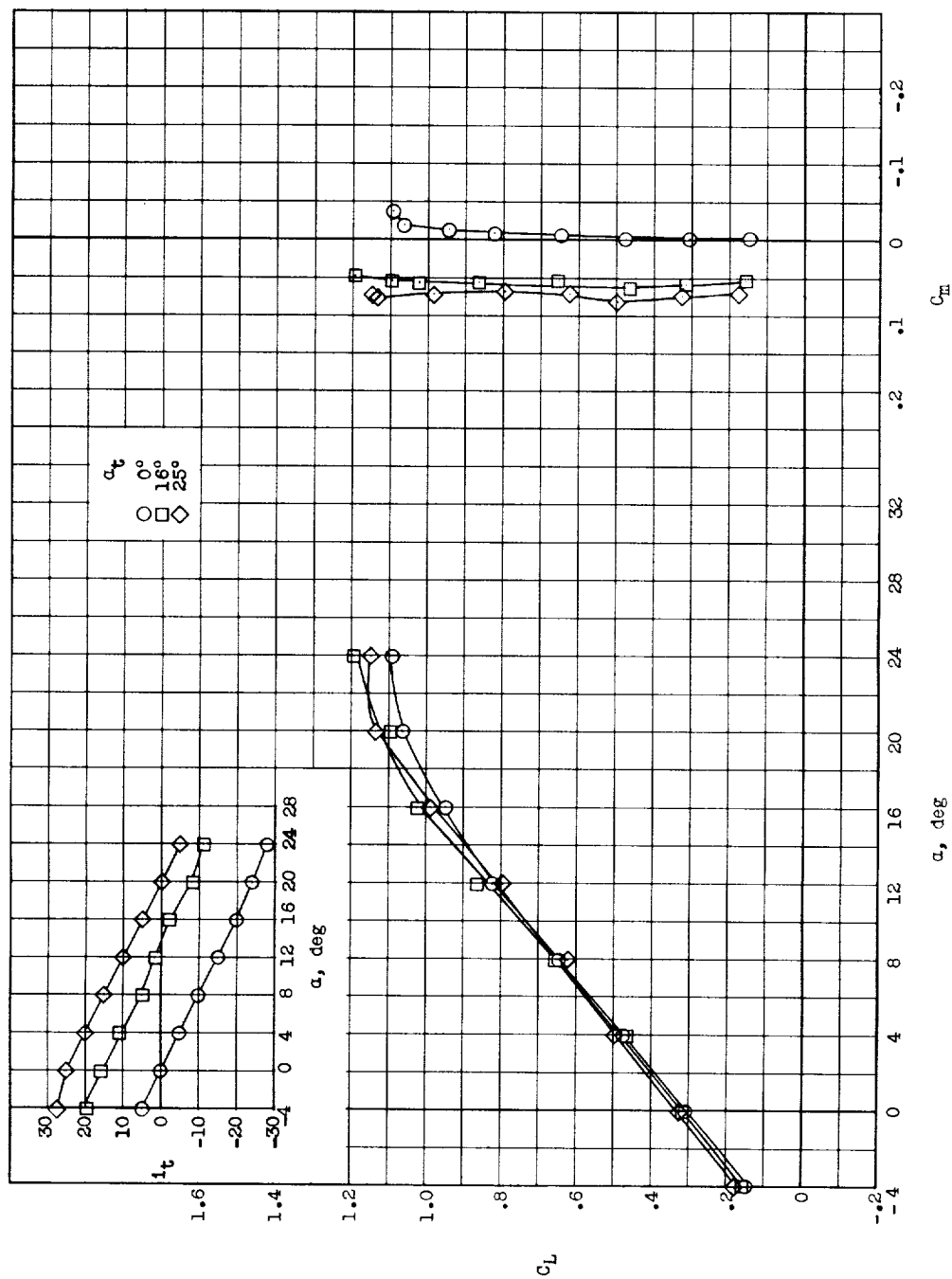
(a) Lift and pitching moment.

Figure 6.- Longitudinal characteristics of model I. $i_w = 8°$; center of gravity located at $0.275\bar{c}$.
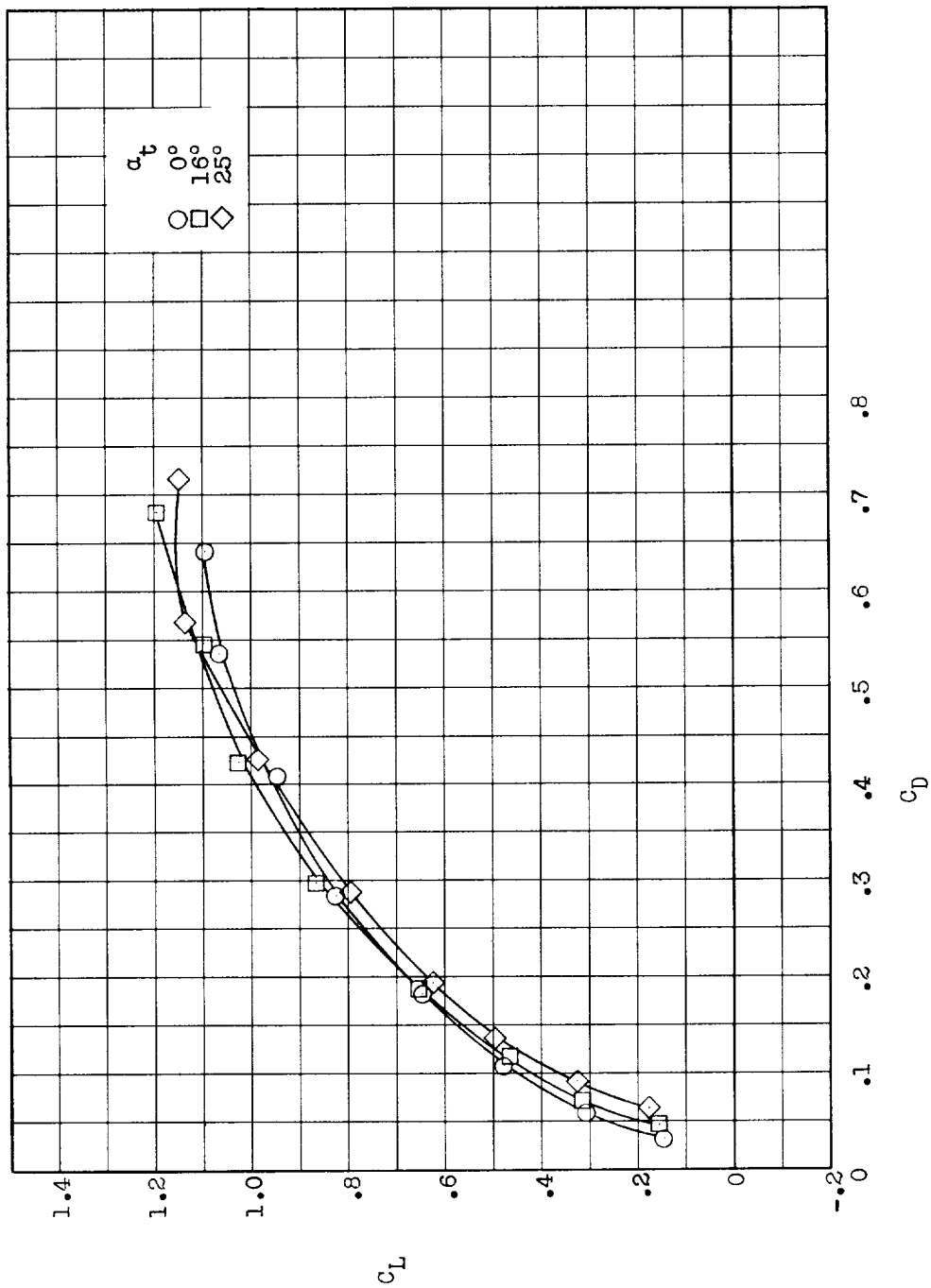
(b) Drag.

Figure 6.- Concluded.

22
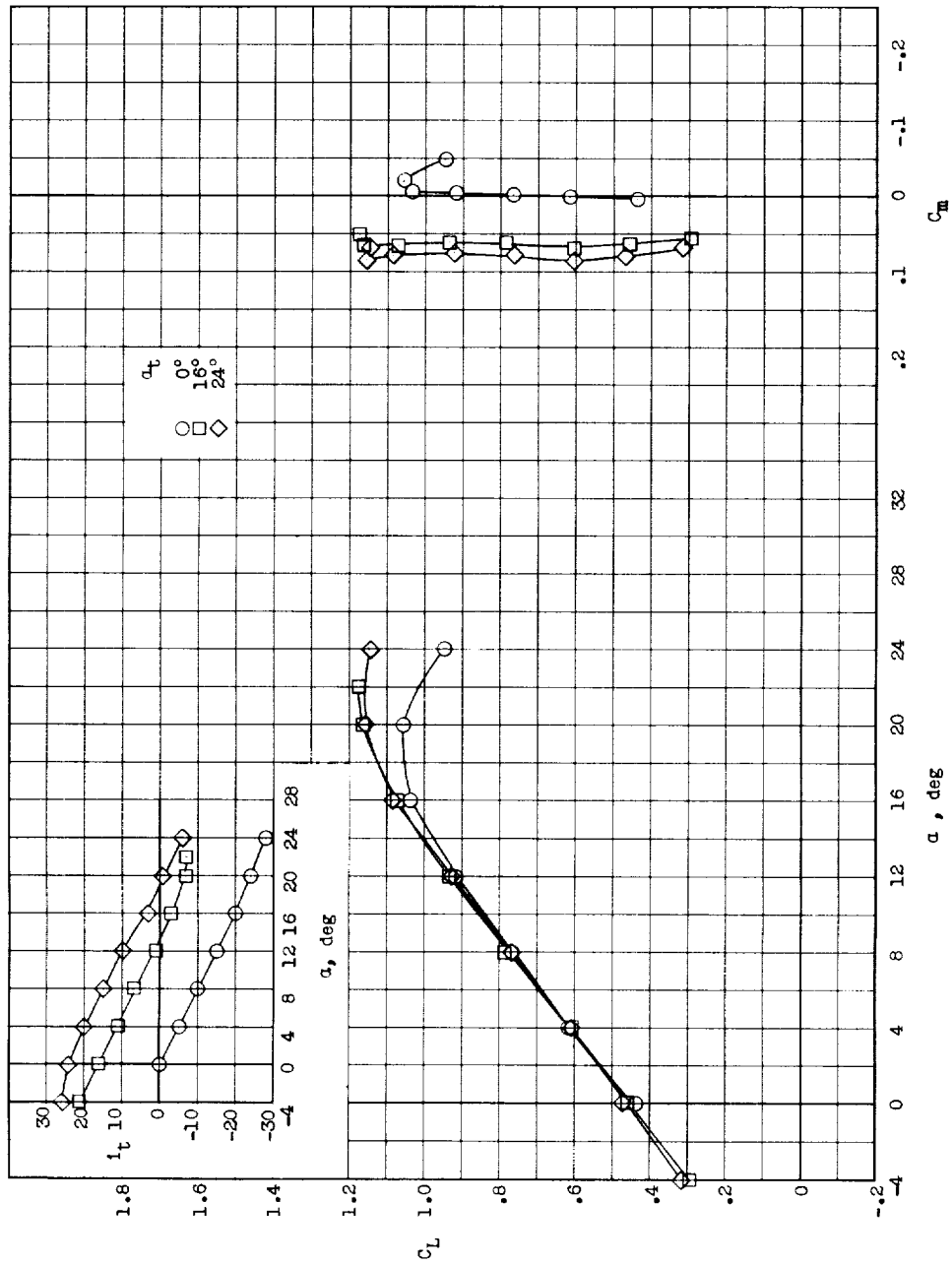
(a) Lift and pitching moment.

Figure 7.- Longitudinal characteristics of model I. $i_w = 12^o$; center of gravity located at $0.275\bar{c}$.
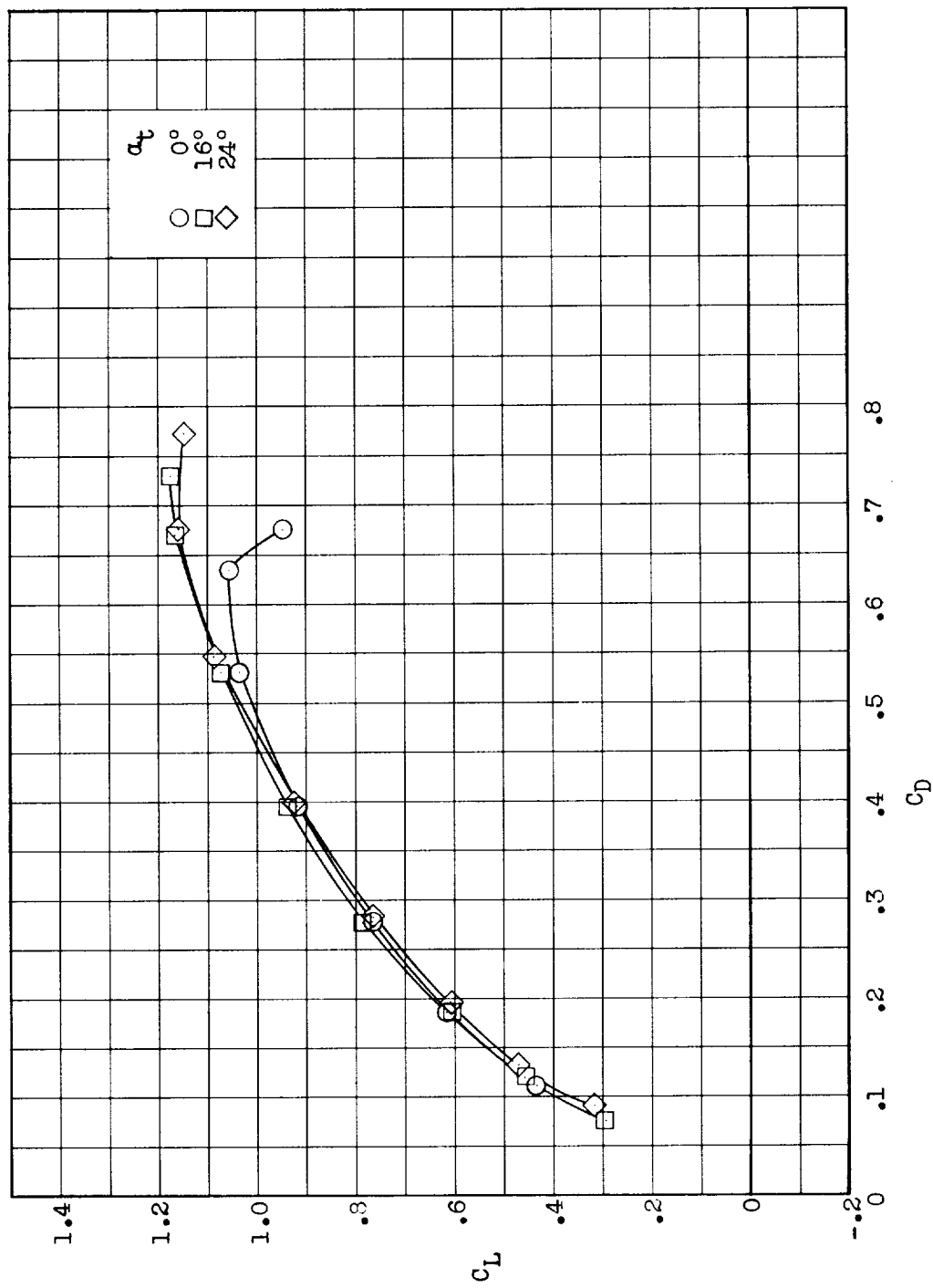
(b) Drag.

Figure 7.- Concluded.
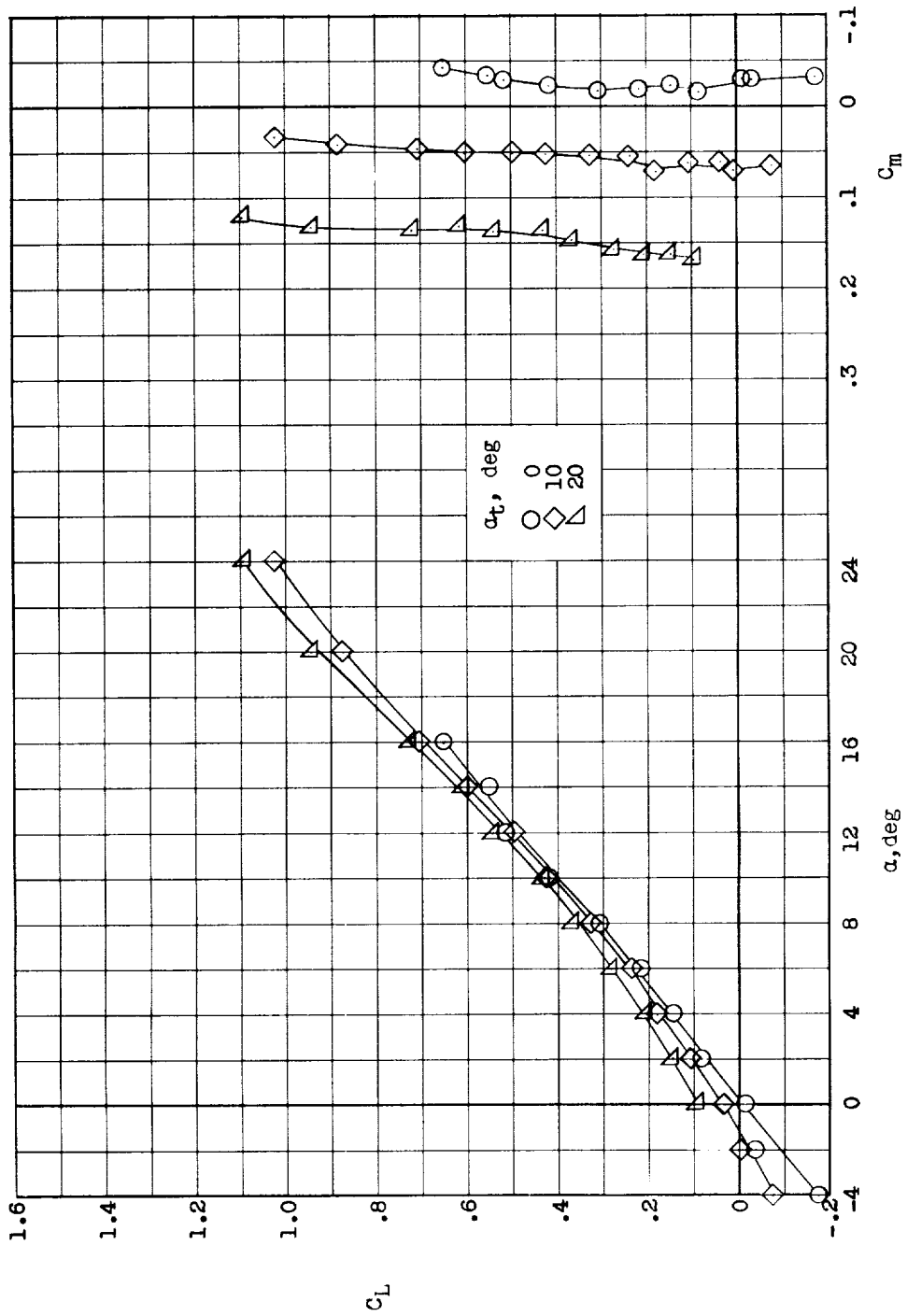
(a) Lift and pitching moment.

Figure 8.- Longitudinal characteristics of model II. $i_w = 0^\circ$; $\delta_f = 0^\circ$; $\delta_{f,t} = 0^\circ$; canard slat deflected; center of gravity located at $0.275\bar{c}$.
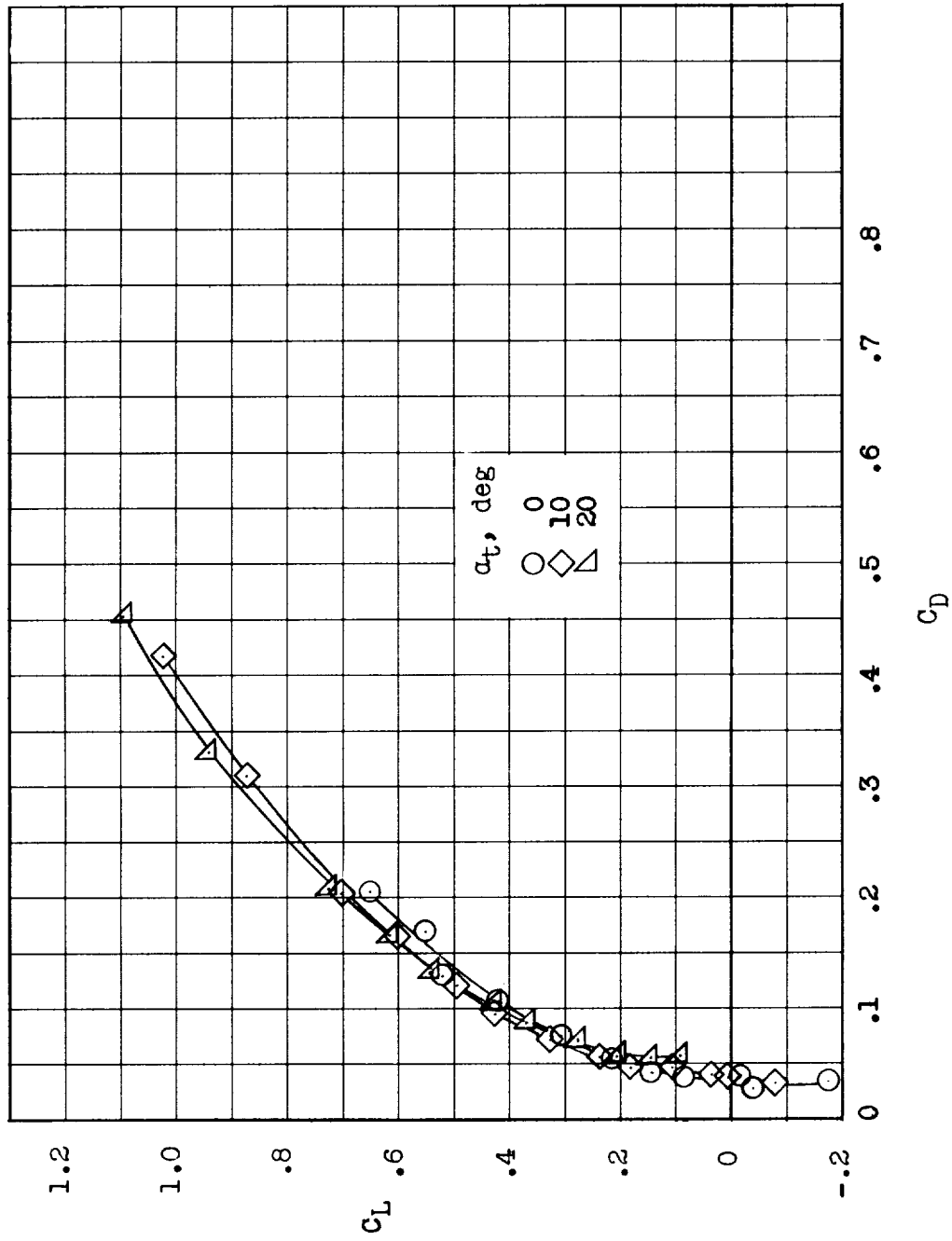
(b) Drag.

Figure 8.- Concluded.
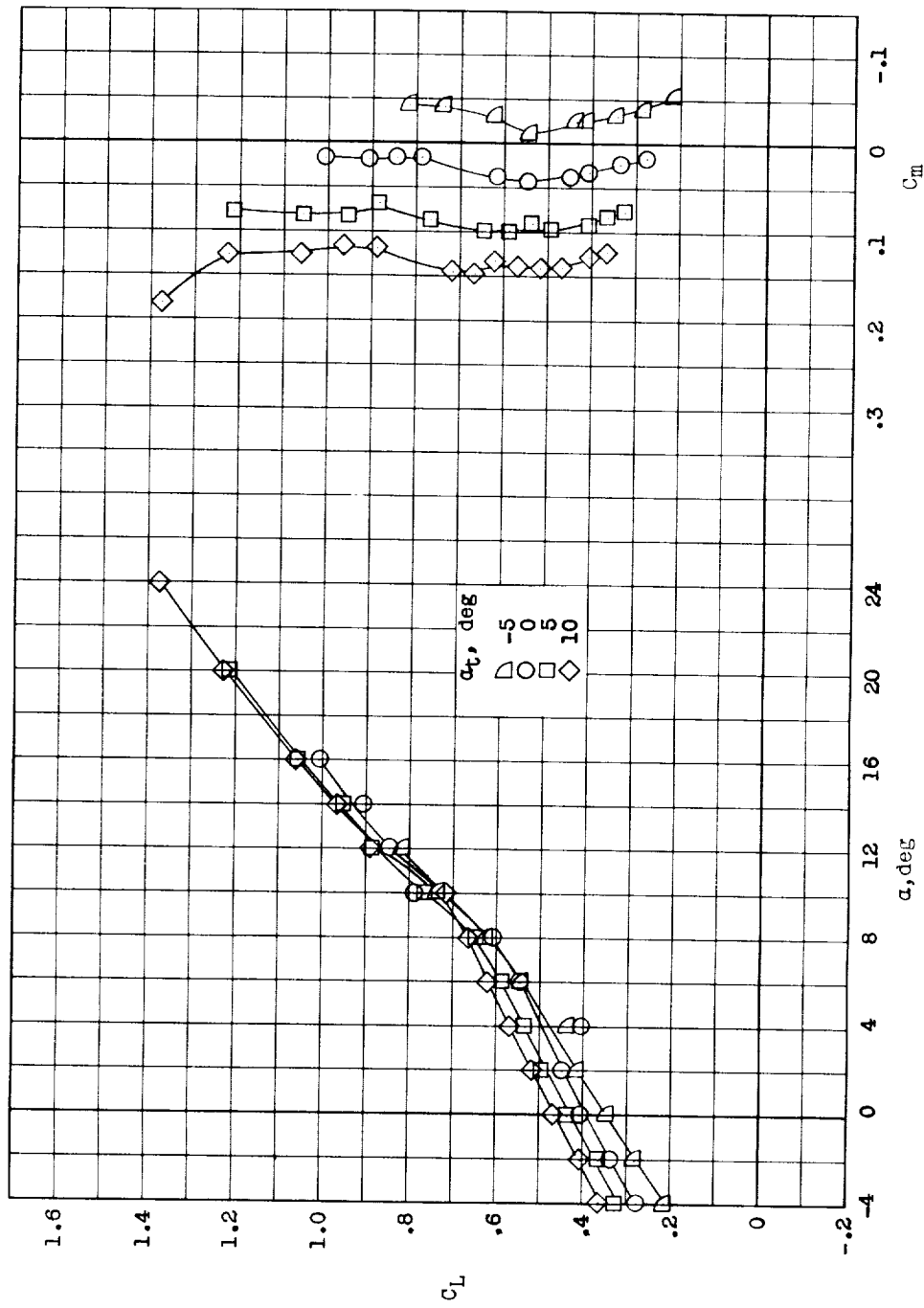
(a) Lift and pitching moment.

Figure 9.- Longitudinal characteristics of model II. $i_w = 0°$; $\delta_f = 30°$; high-lift canard, $C_{\mu,t} = 0.031$; center of gravity located at $0.275\bar{c}$.
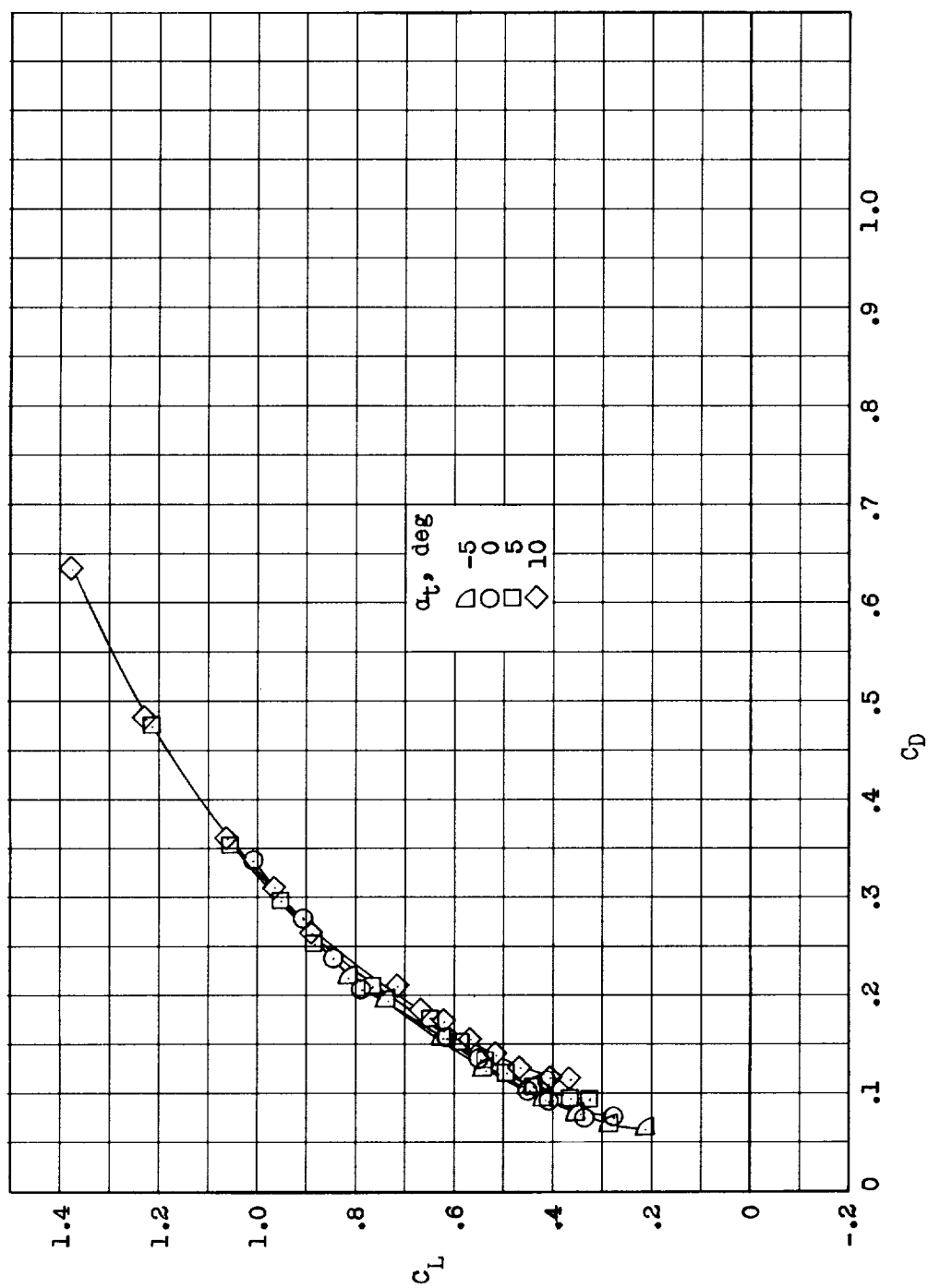
(b) Drag.

Figure 9.- Concluded.
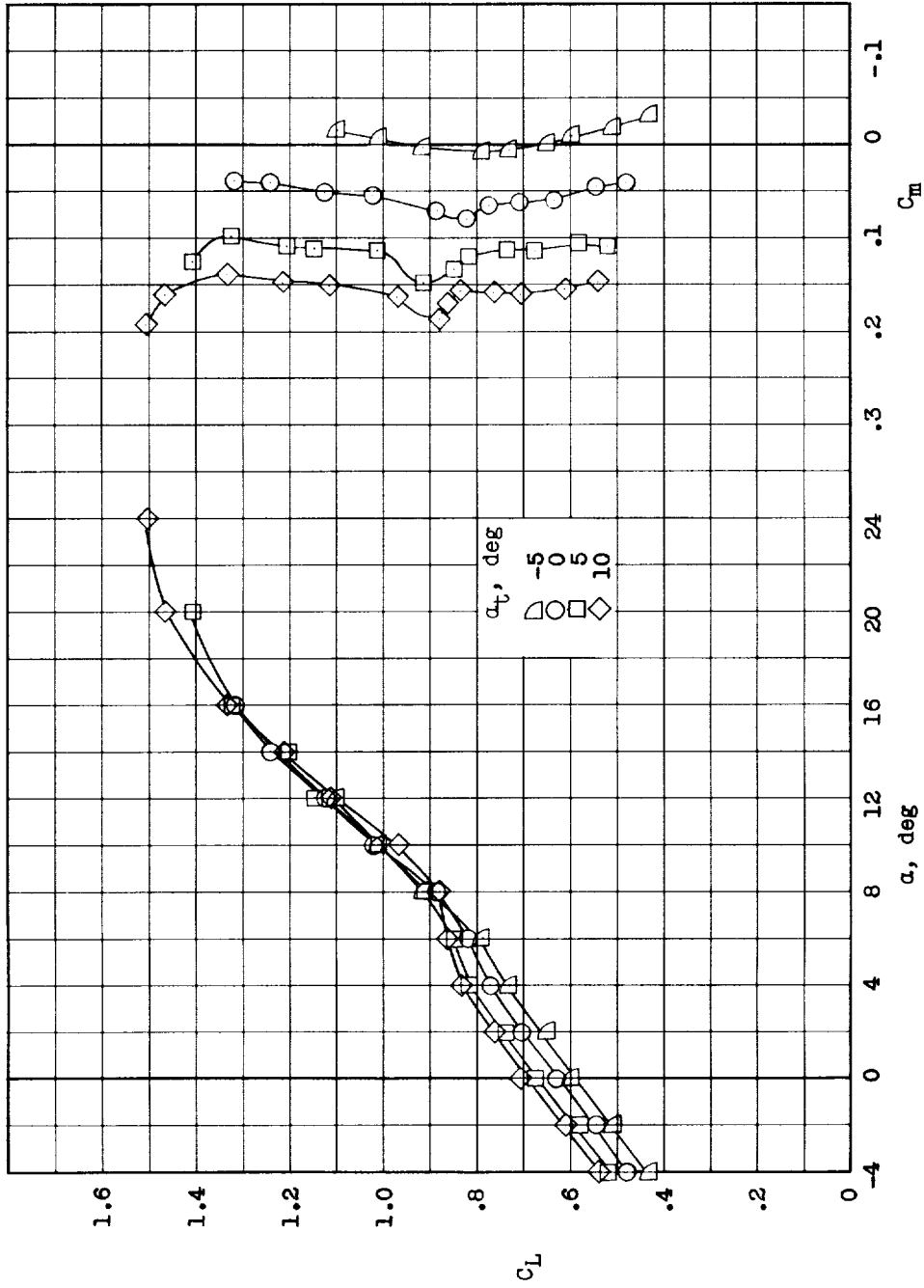
(a) Lift and pitching moment.

Figure 10.- Longitudinal characteristics of model II. $i_w = 8^o$; $\delta_f = 30^o$; high-lift canard, $C_{\mu,t} = 0.031$; center of gravity located at $0.275\bar{c}$.
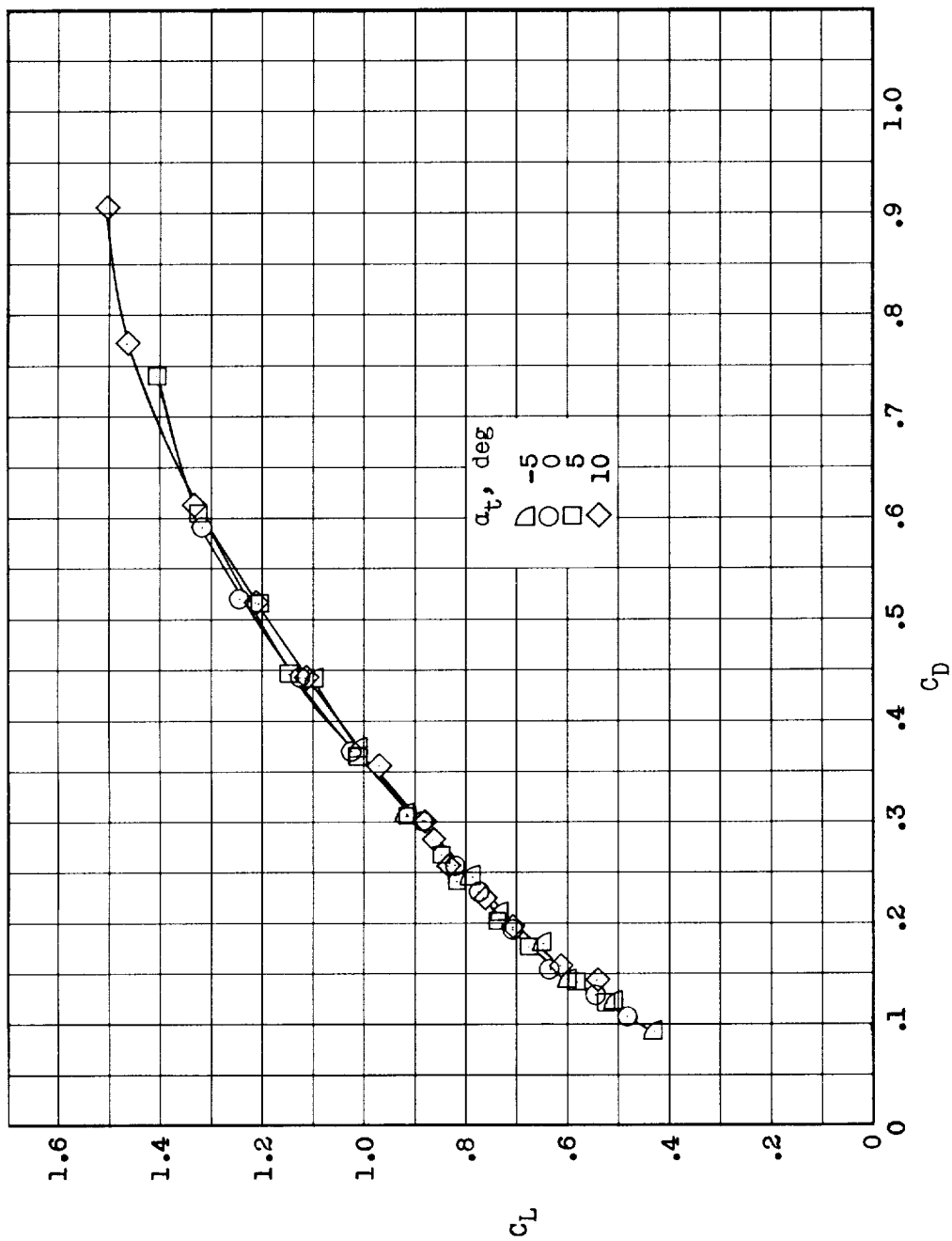
(b) Drag.

Figure 10.- Concluded.
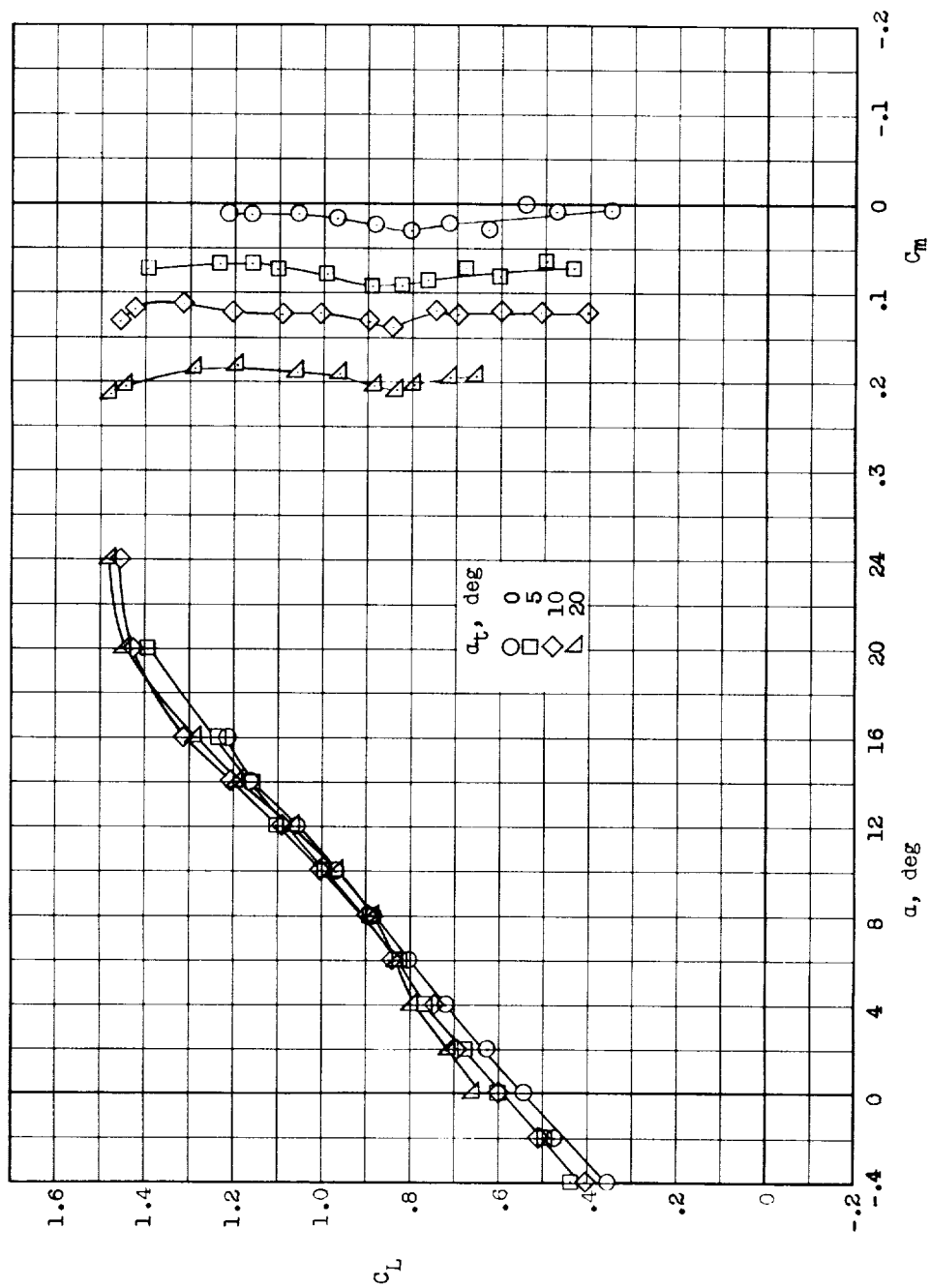
(a) Lift and pitching moment.

Figure 11.- Longitudinal characteristics of model II. $i_w = 12°$; $\delta_f = 10°$; high-lift canard, $C_{\mu,t} = 0$; center of gravity located at $0.275\bar{c}$.
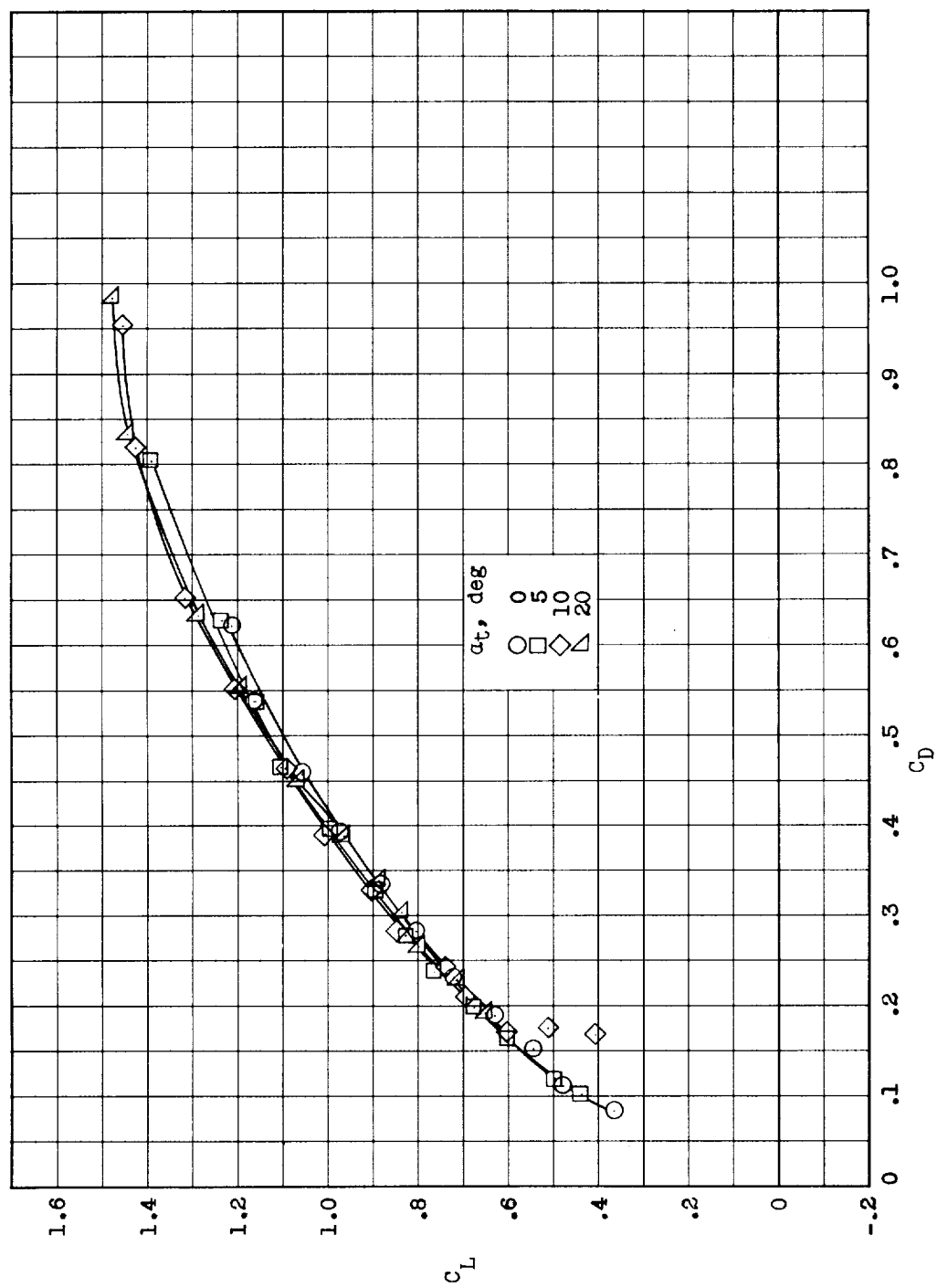
(b) Drag.

Figure 11.- Concluded.
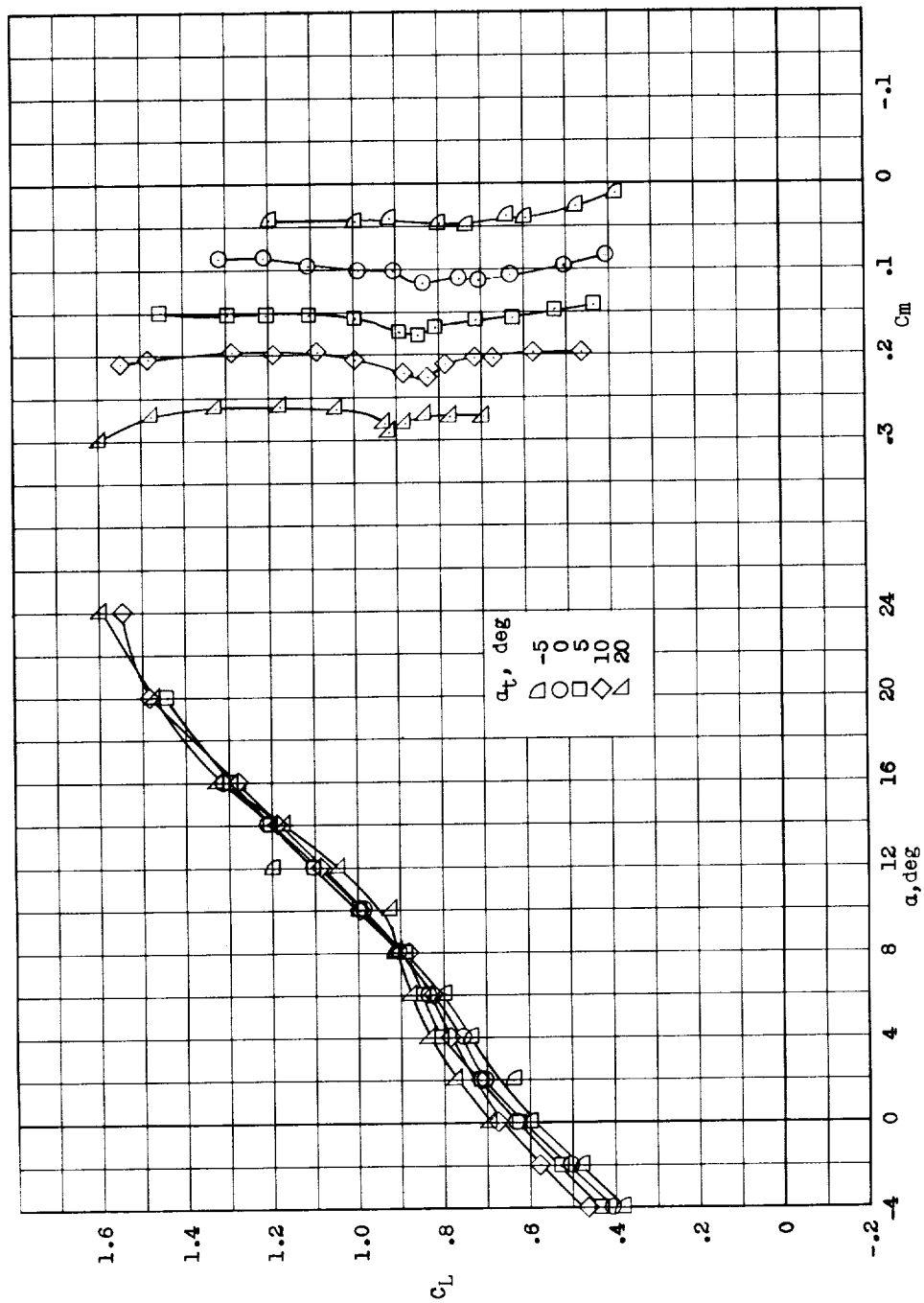
(a) Lift and pitching moment.

Figure 12.- Longitudinal characteristics of model II. $i_w = 12^o$; $\delta_f = 10^o$; high-lift canard, $C_{\mu,t} = 0.025$; center of gravity located at $0.275\bar{c}$.
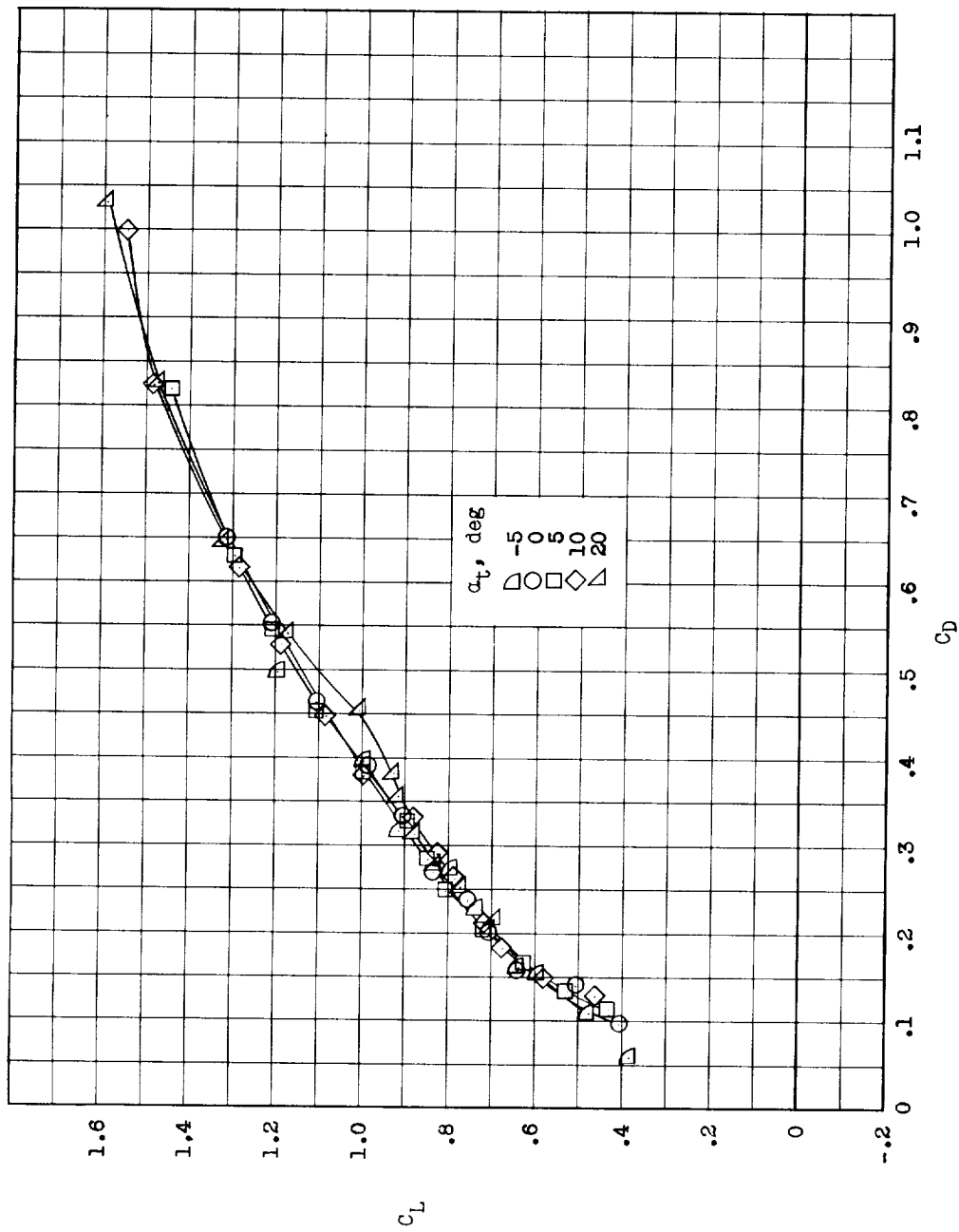
(b) Drag.

Figure 12.- Concluded.
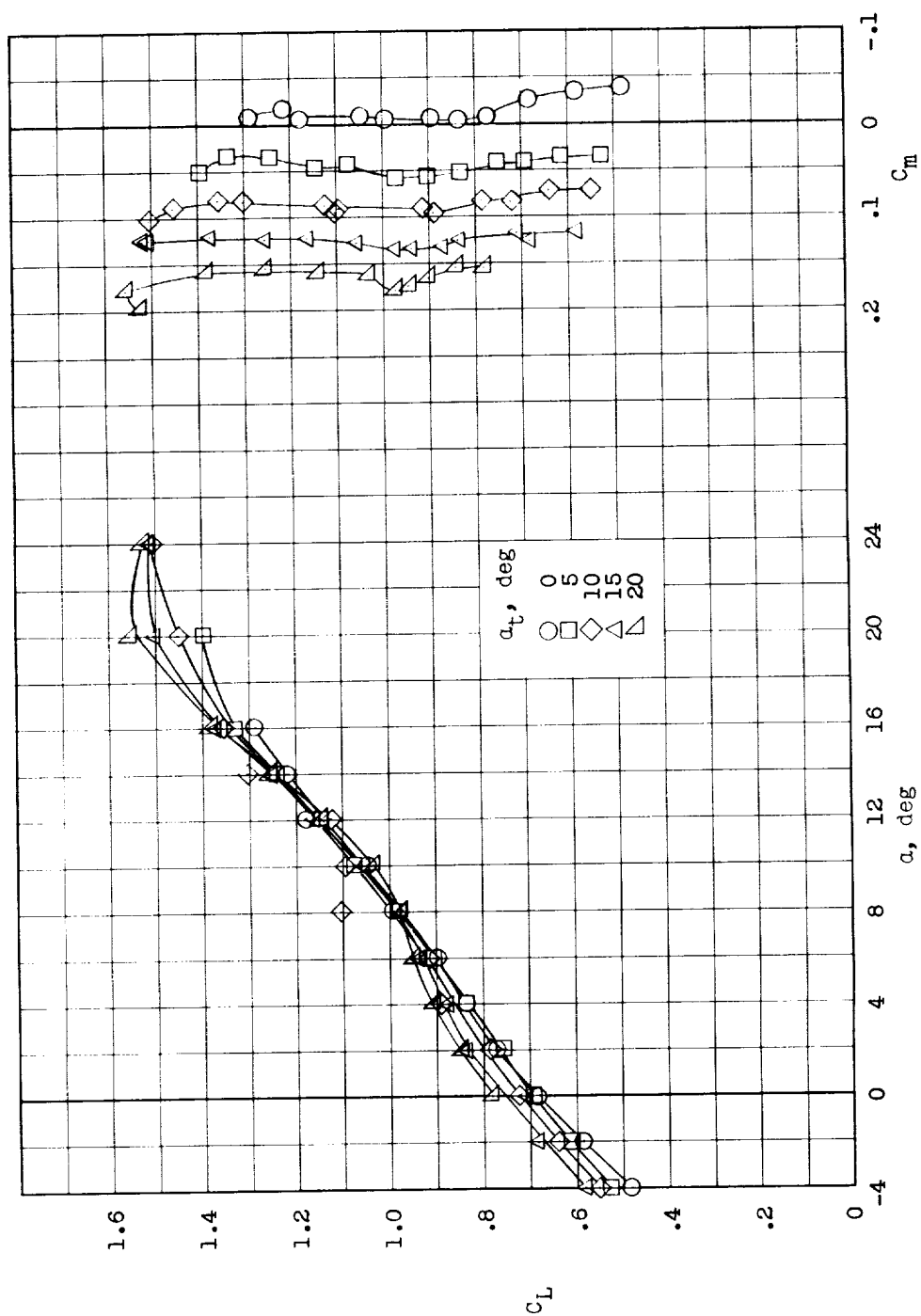
(a) Lift and pitching moment.

Figure 13.- Longitudinal characteristics of model II. $i_w = 12°$; $\delta_f = 20°$; high-lift canard, $C_{\mu,t} = 0$; center of gravity located at $0.275\bar{c}$.
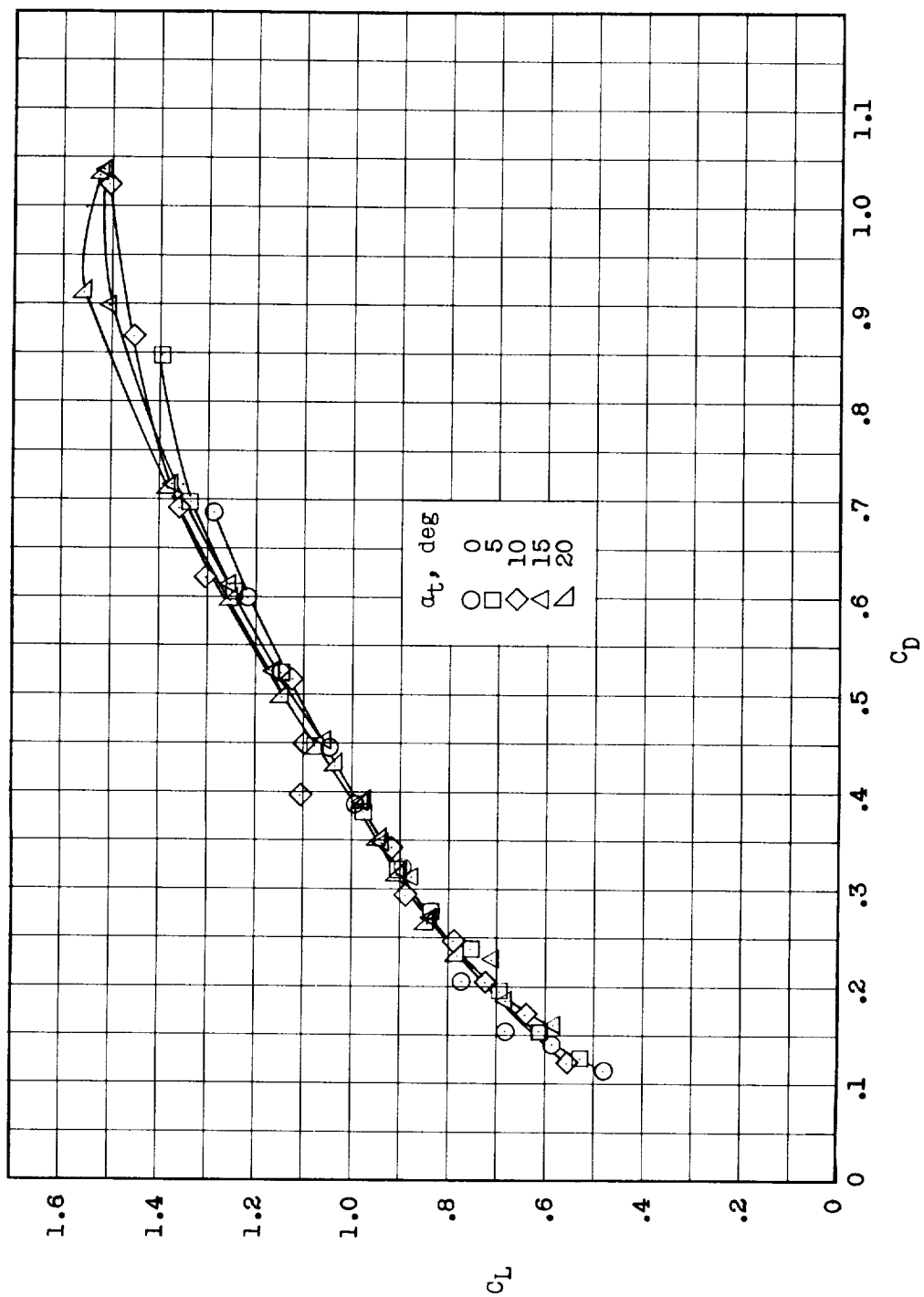
(b) Drag.

Figure 13.- Concluded.
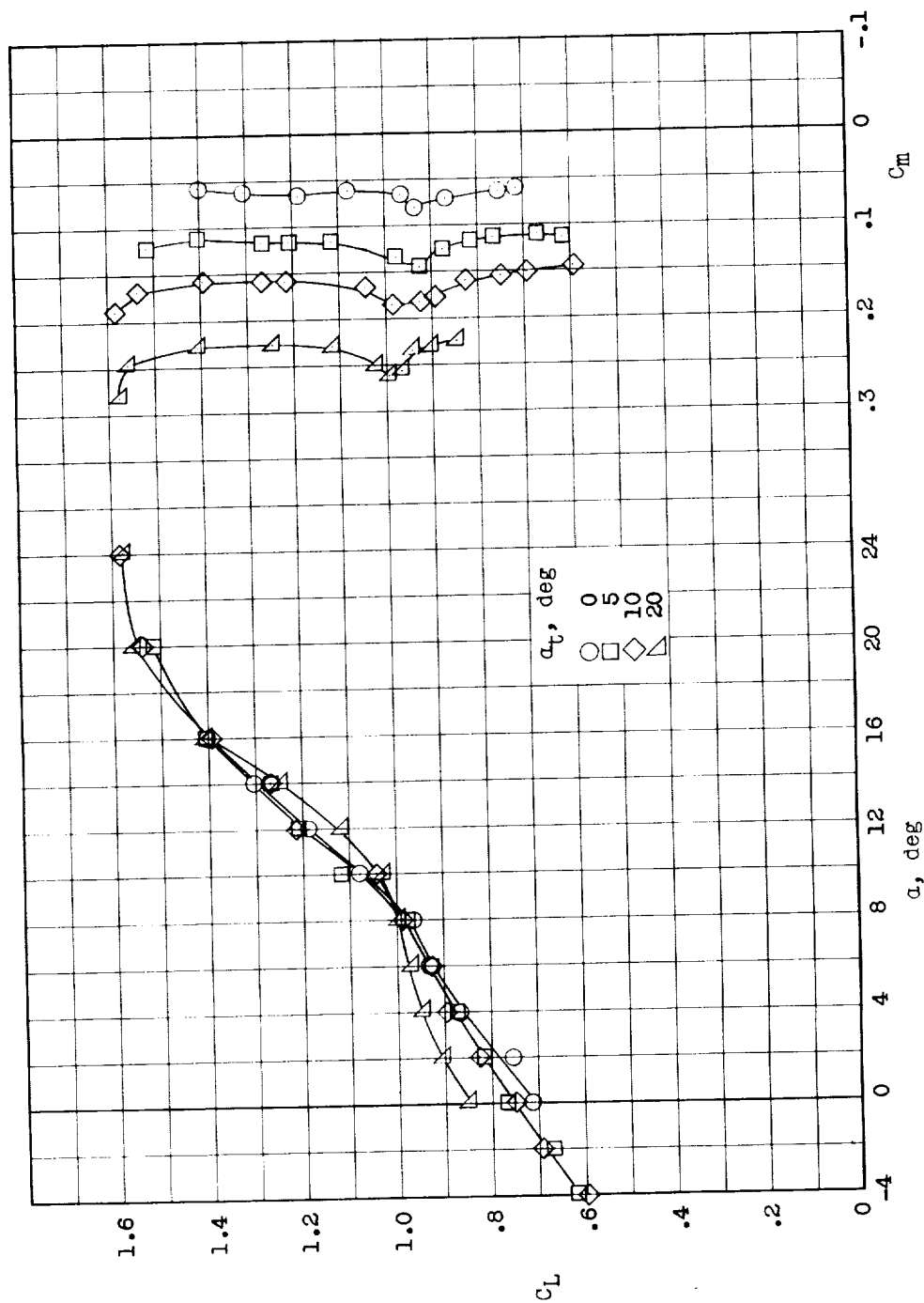
(a) Lift and pitching moment.

Figure 14.- Longitudinal characteristics of model II. $i_w = 12^\circ$; $\delta_f = 20^\circ$; high-lift canard, $C_{\mu,t} = 0.025$; center of gravity located at $0.275\bar{c}$.
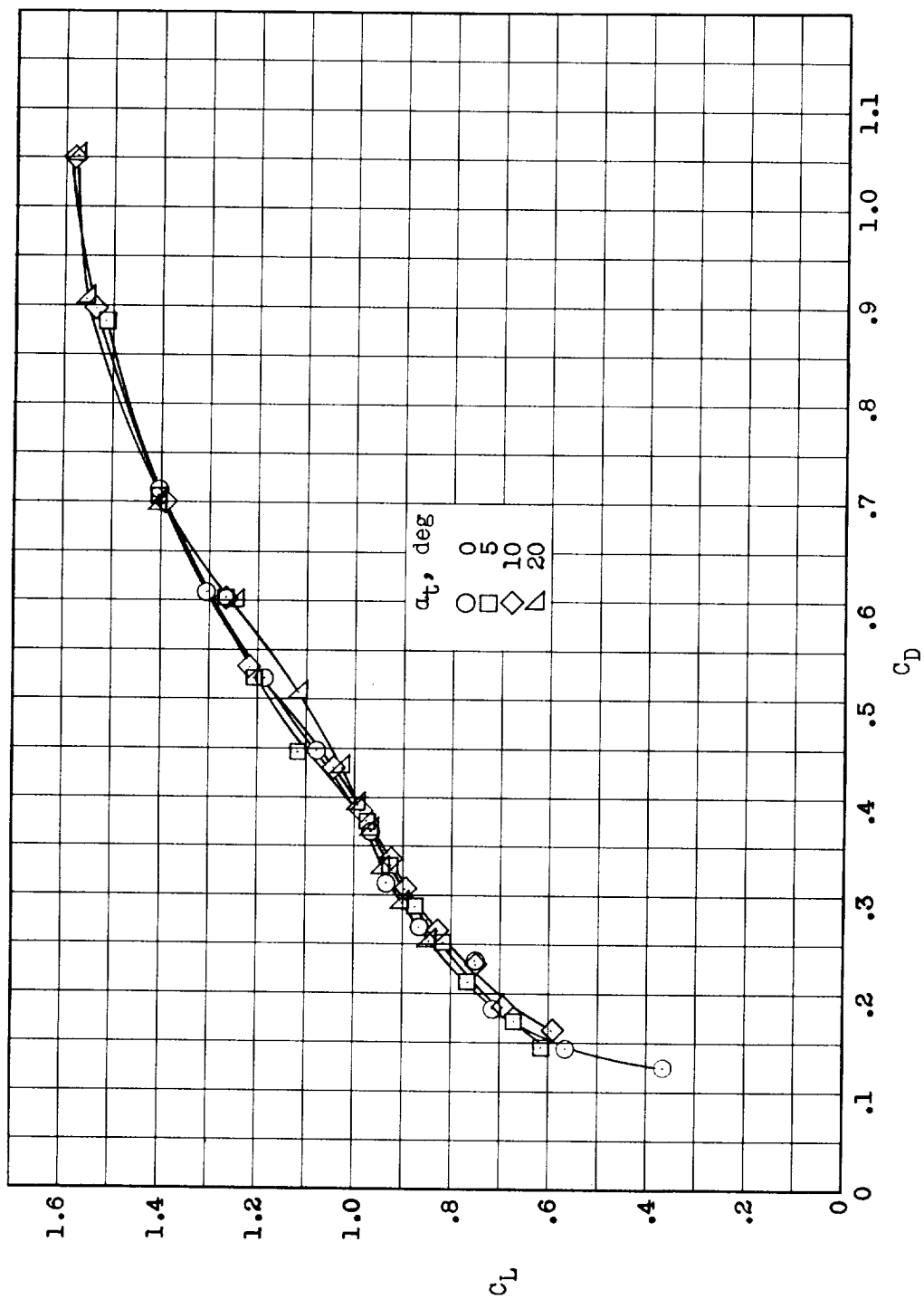
(b) Drag.

Figure 14.- Concluded.

38
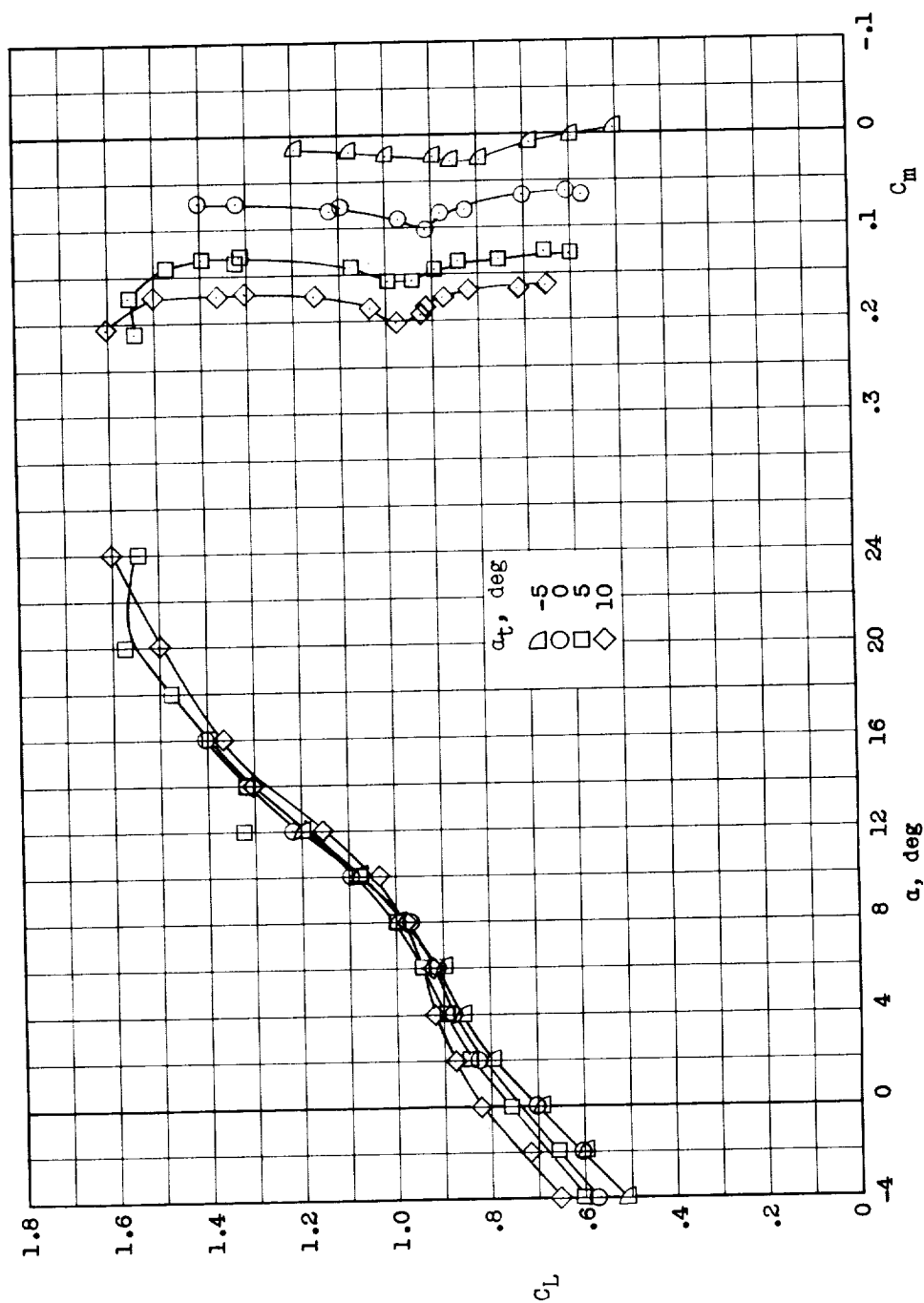
(a) Lift and pitching moment.

Figure 15.- Longitudinal characteristics of model II. $i_w = 12°$; $\delta_f = 20°$; high-lift canard, $C_{\mu,t} = 0.031$; center of gravity located at $0.275\bar{c}$.
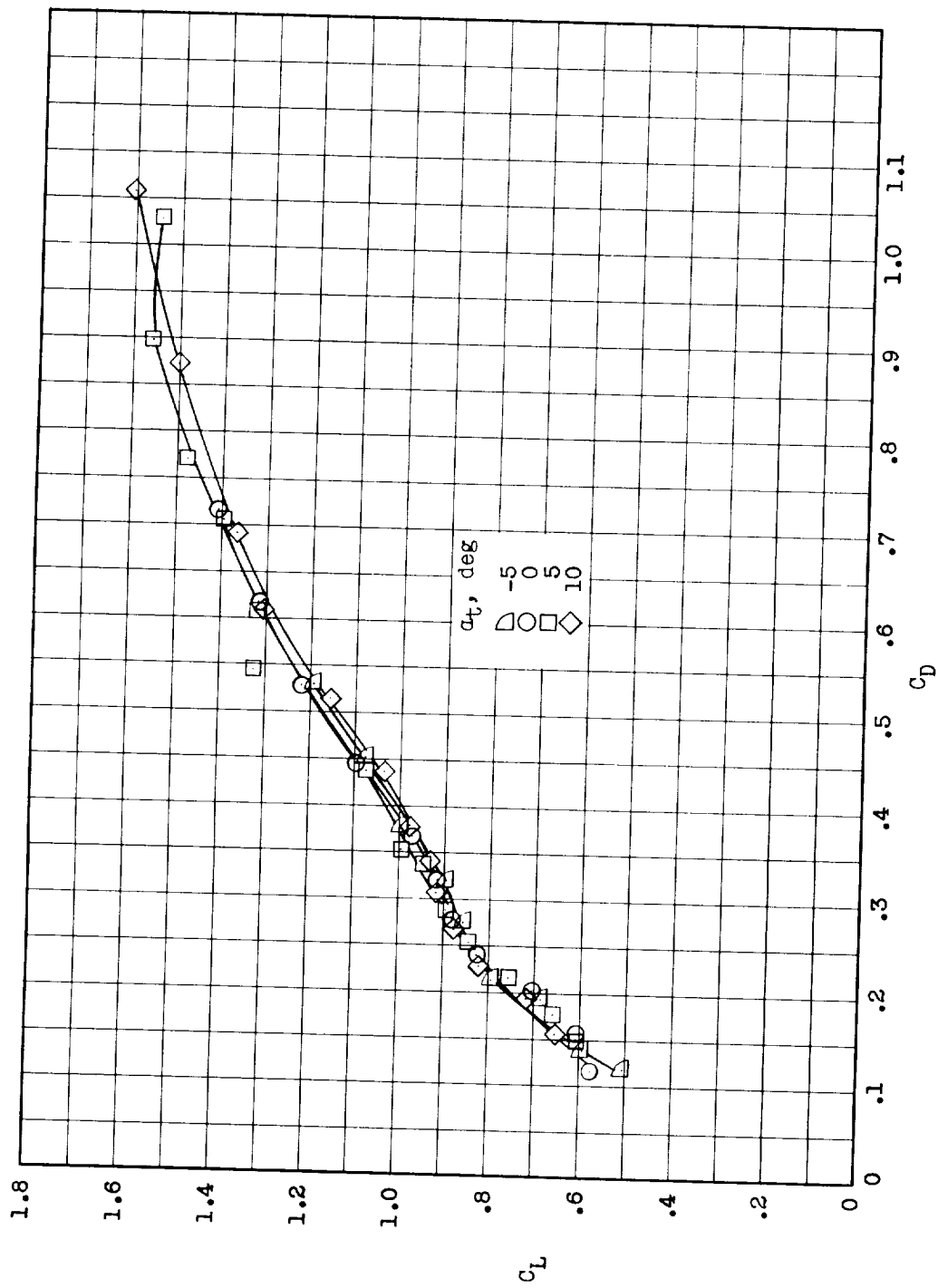
(b) Drag.

Figure 15.- Concluded.
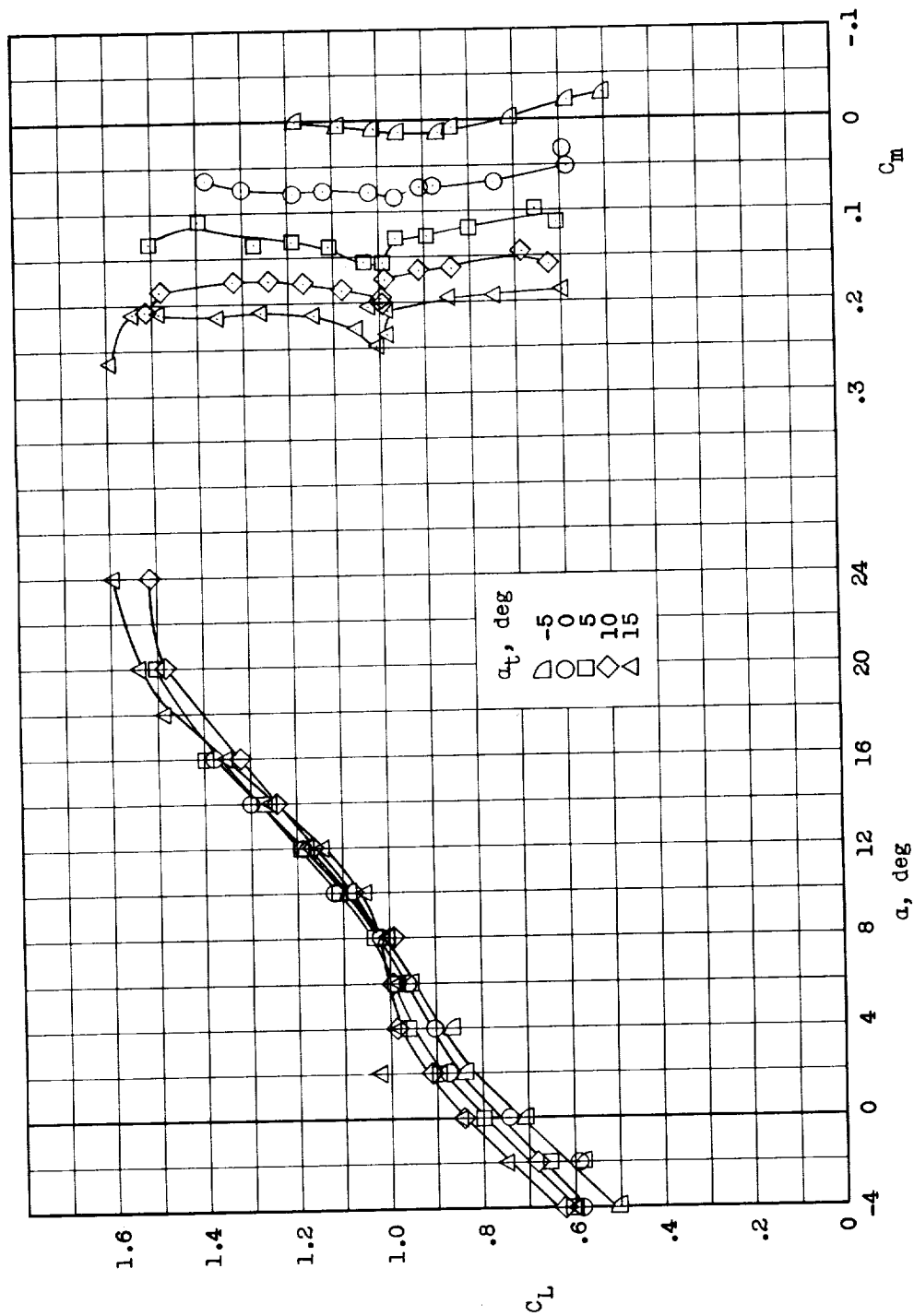
(a) Lift and pitching moment.

Figure 16.- Longitudinal characteristics of model II. $i_w = 12^\circ$; $\delta_f = 30^\circ$; high-lift canard, $C_{\mu,t} = 0.031$; center of gravity located at $0.275\bar{c}$.
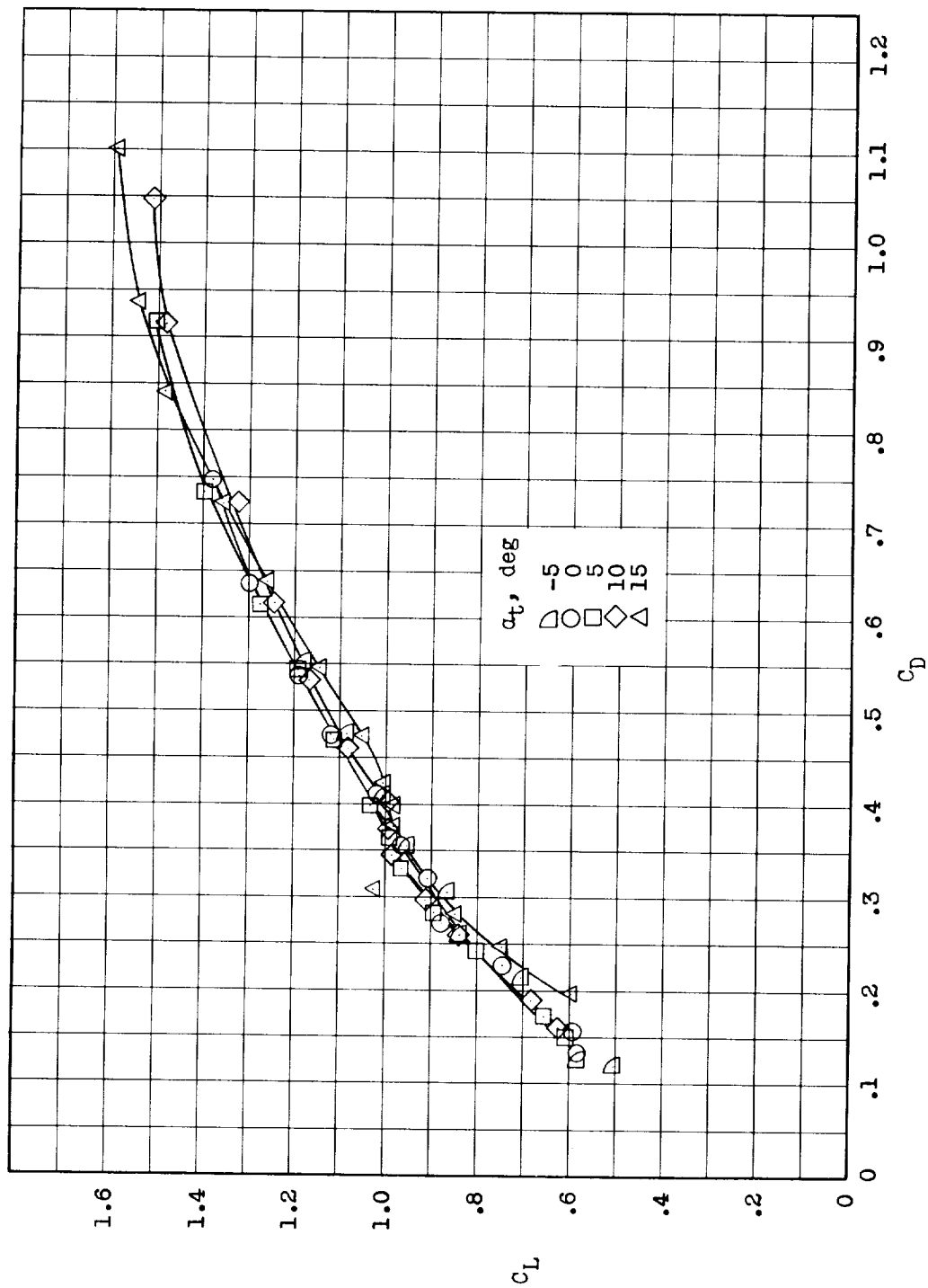
(b) Drag.

Figure 16.- Concluded.
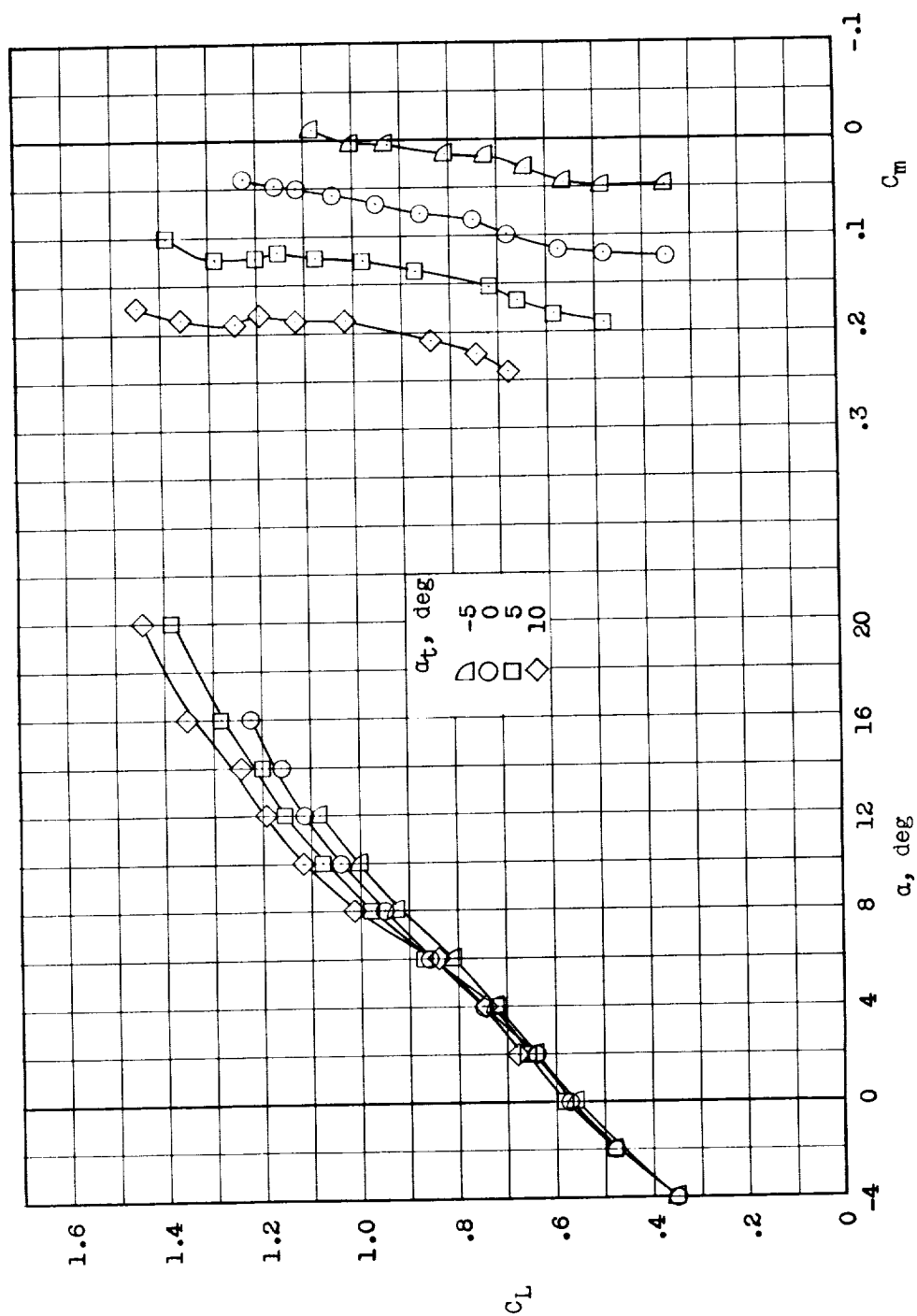
(a) Lift and pitching moment.

Figure 17.- Longitudinal characteristics of model II. $i_w = 12^\circ$; $\delta_f = 10^\circ$; high-lift canard in high position, $C_{\mu,t} = 0.025$; center of gravity located at $0.275\bar{c}$.
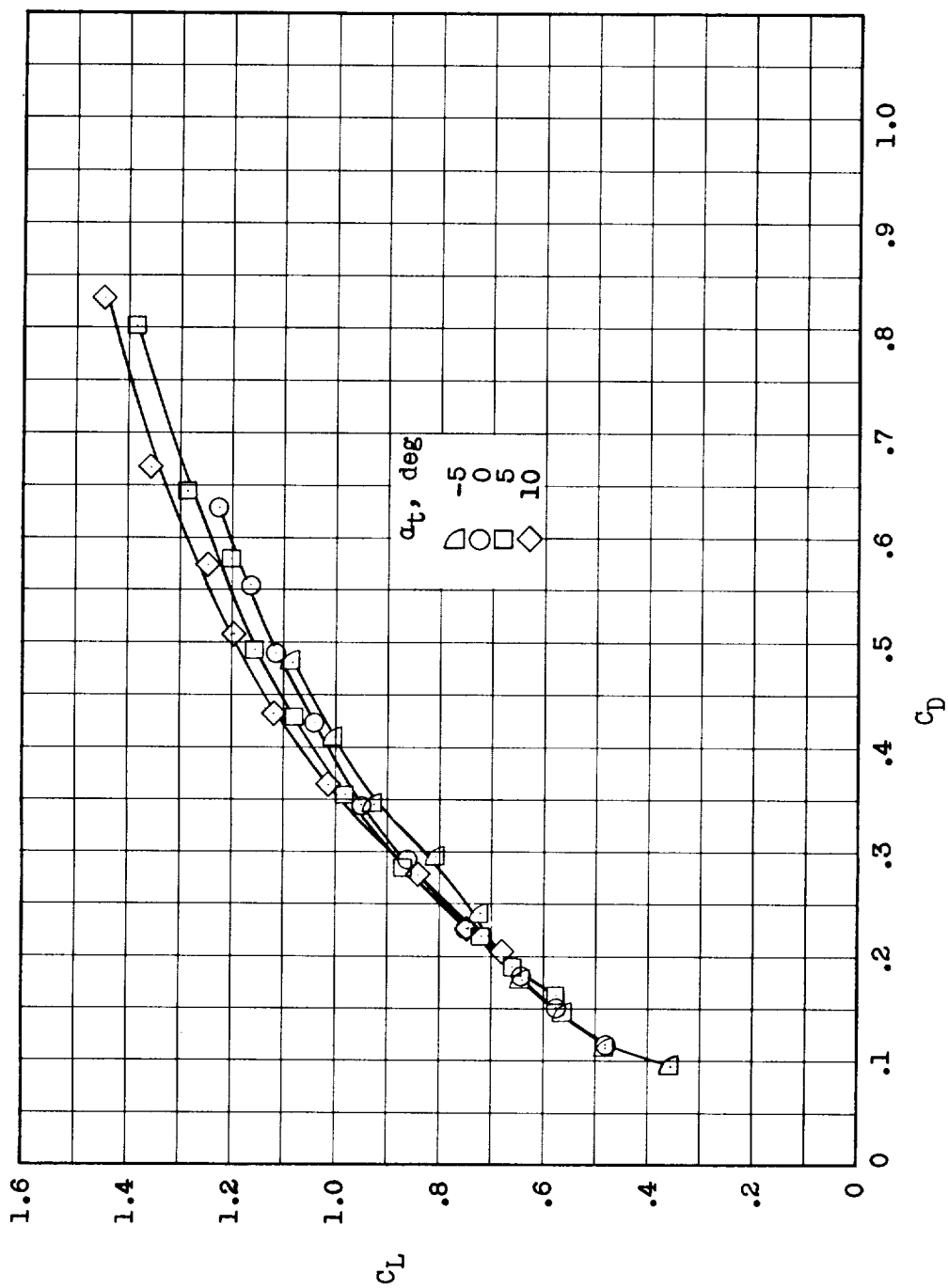
(b) Drag.

Figure 17.- Concluded.
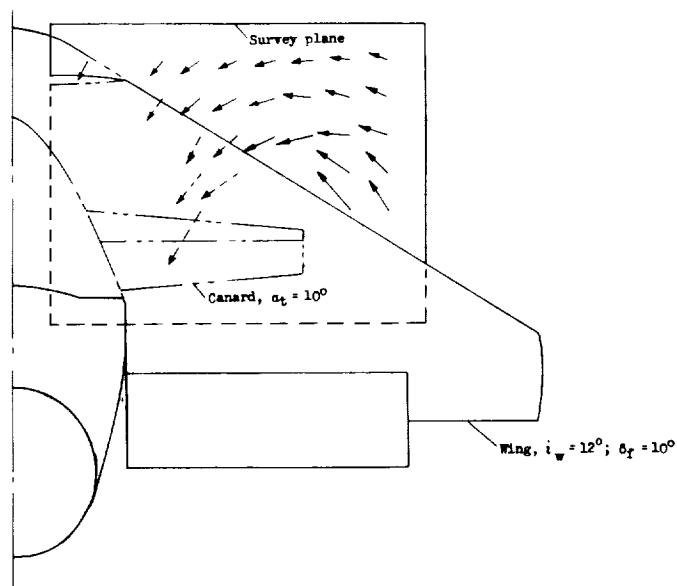
(a) Canard in low position.
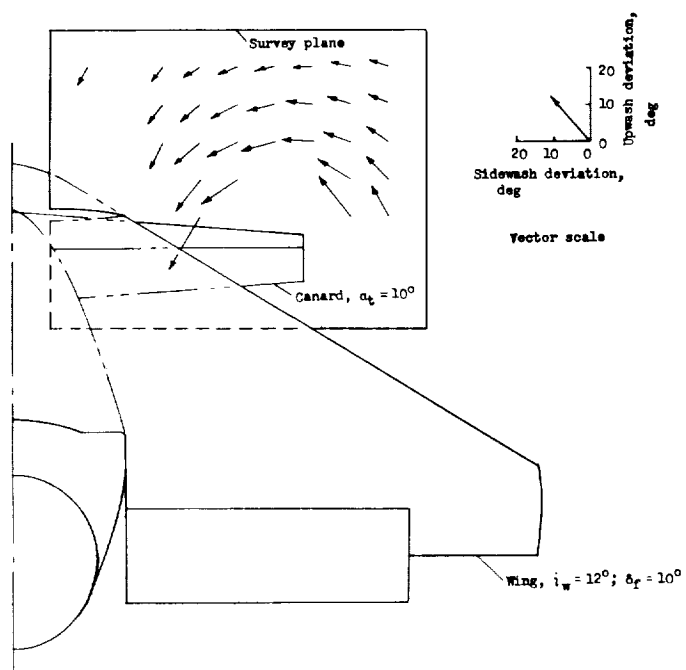
(b) Canard in high position.

Figure 18.- Flow field behind the high-lift canard in relation to the wing for two canard positions. $\alpha = 8°$; $C_{\mu,t} = 0.025$. View from behind in direction of free-stream flow.
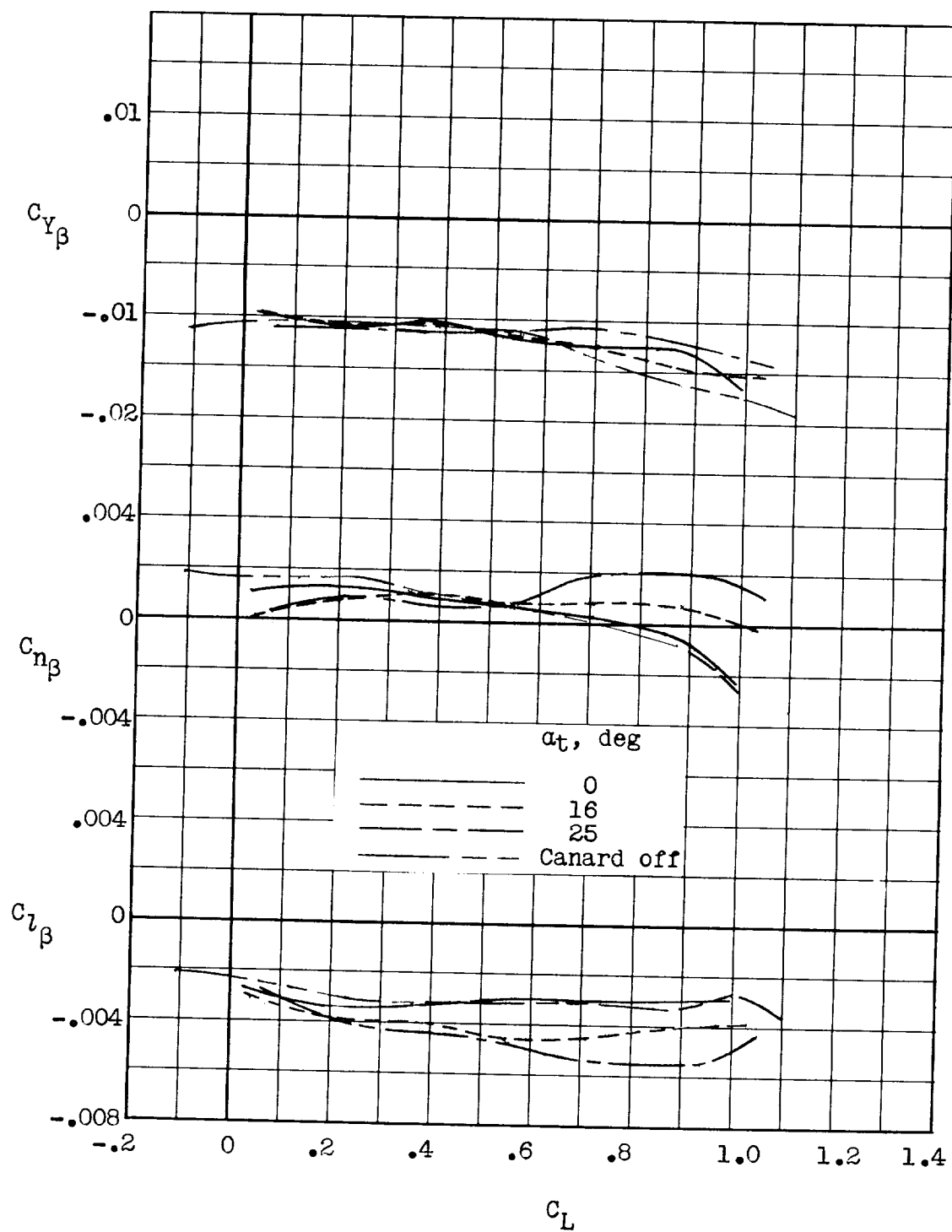
Figure 19.- Lateral characteristics of model I. $i_w = 0^o$; center of gravity located at $0.275\bar{c}$.
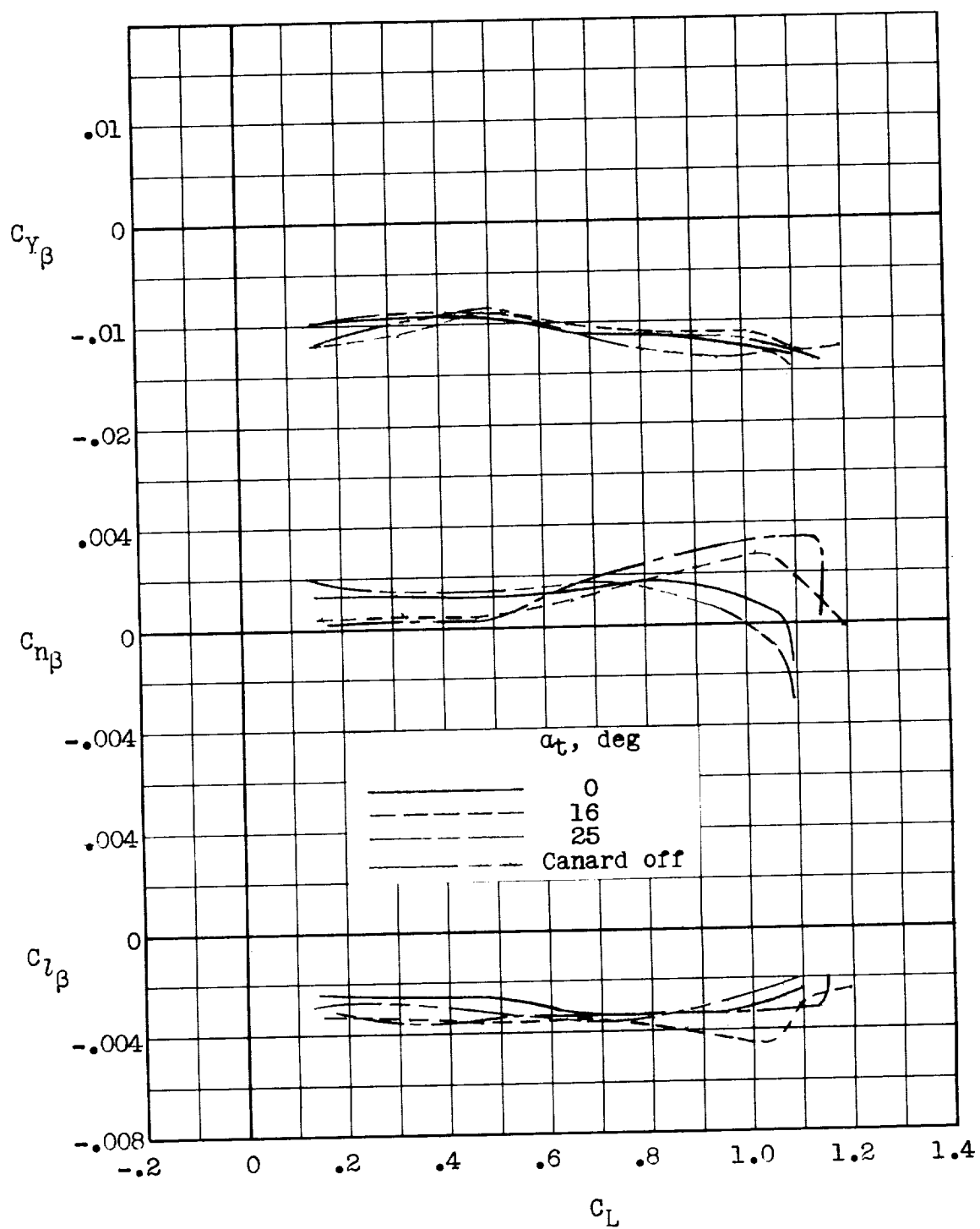
Figure 20.- Lateral characteristics of model I. $i_w = 8°$; center of gravity located at $0.275\bar{c}$.
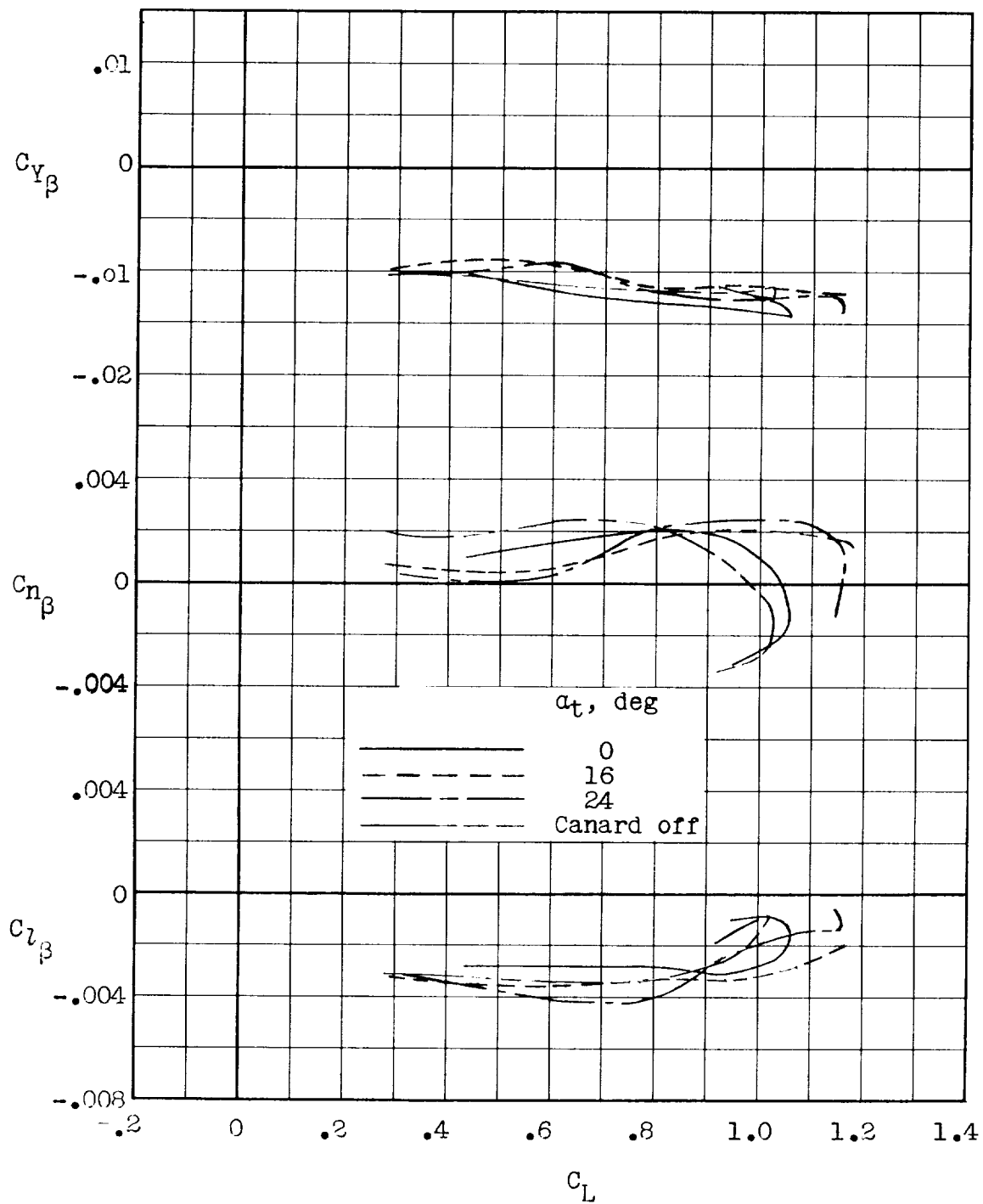
Figure 21.- Lateral characteristics of model I. $i_w = 12°$; center of gravity located at $0.275\bar{c}$.
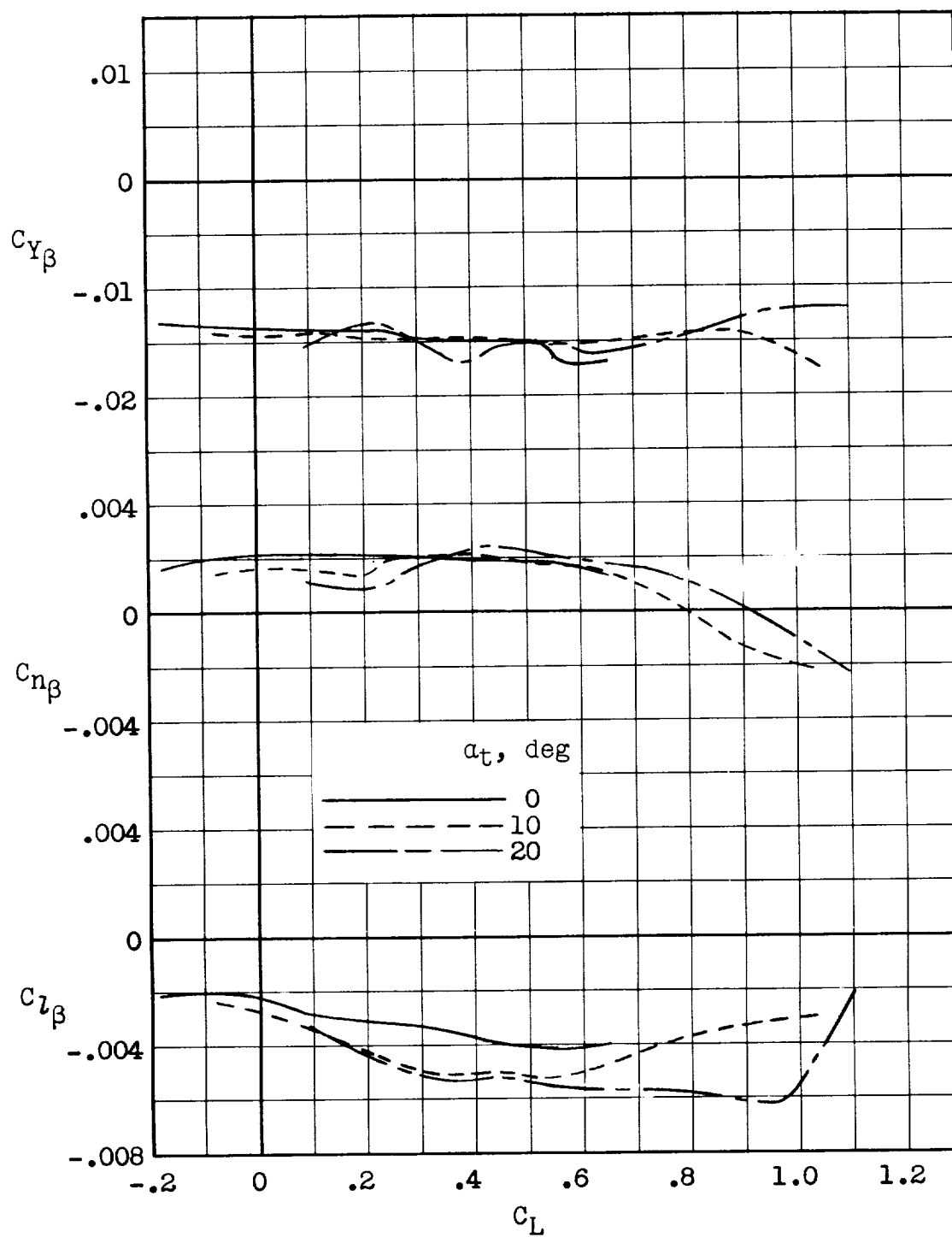
Figure 22.- Lateral characteristics of model II. $i_w = 0^o$; $\delta_f = 0^o$; basic canard; center of gravity located at $0.275\bar{c}$.
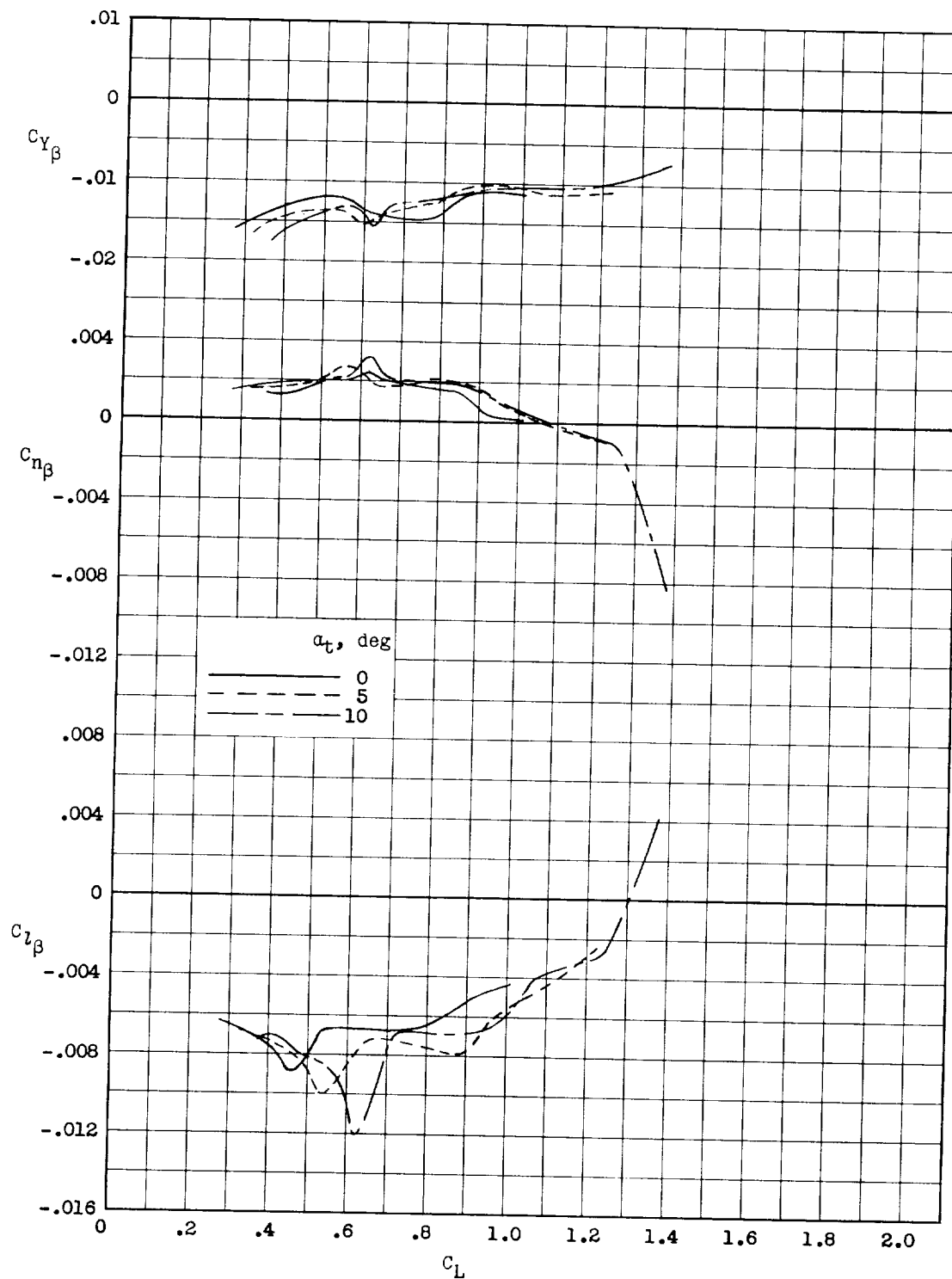
Figure 23.- Lateral characteristics of model II. $i_w = 0°$; $\delta_f = 30°$; high-lift canard, $C_{\mu,t} = 0.031$; center of gravity located at $0.275\bar{c}$.
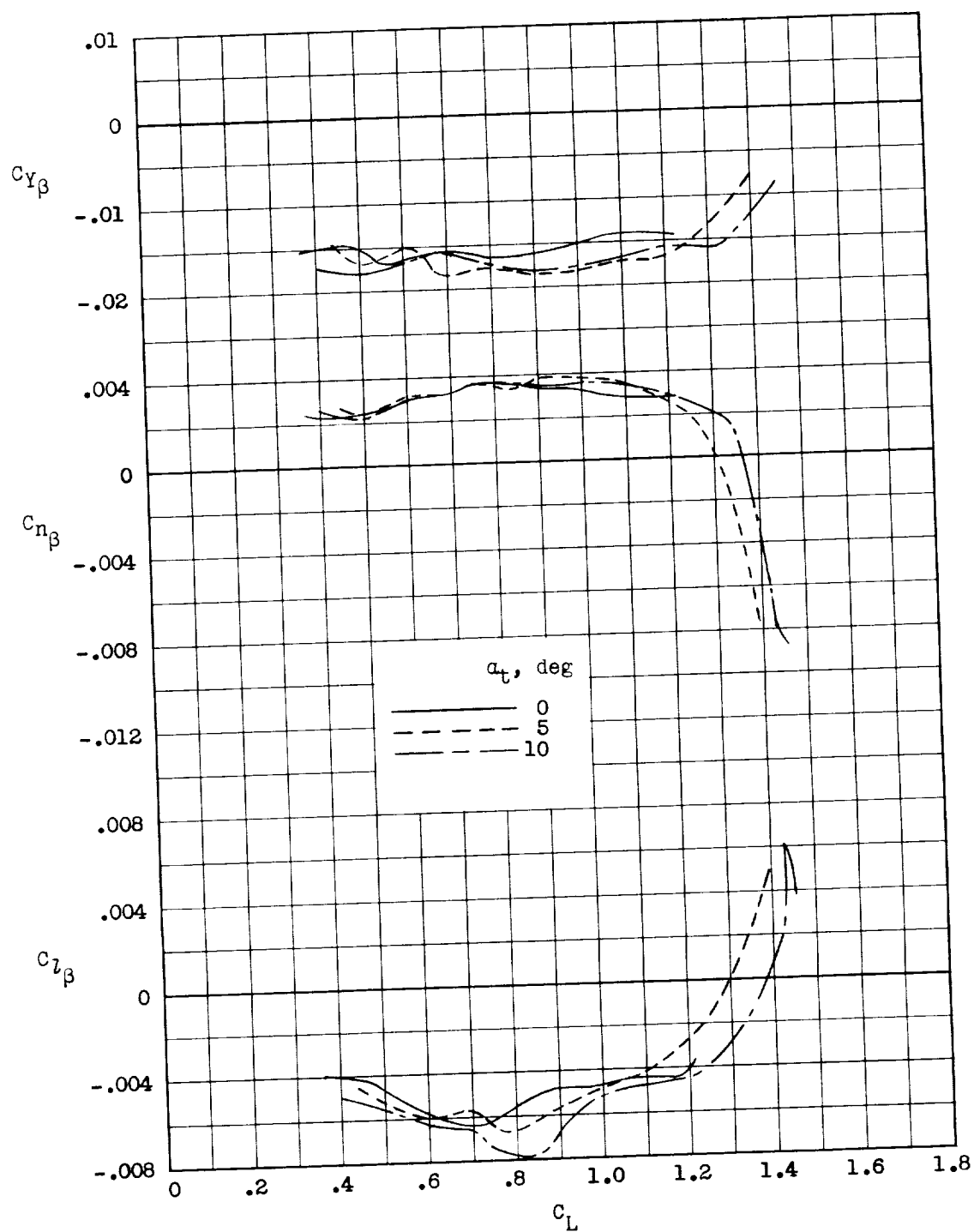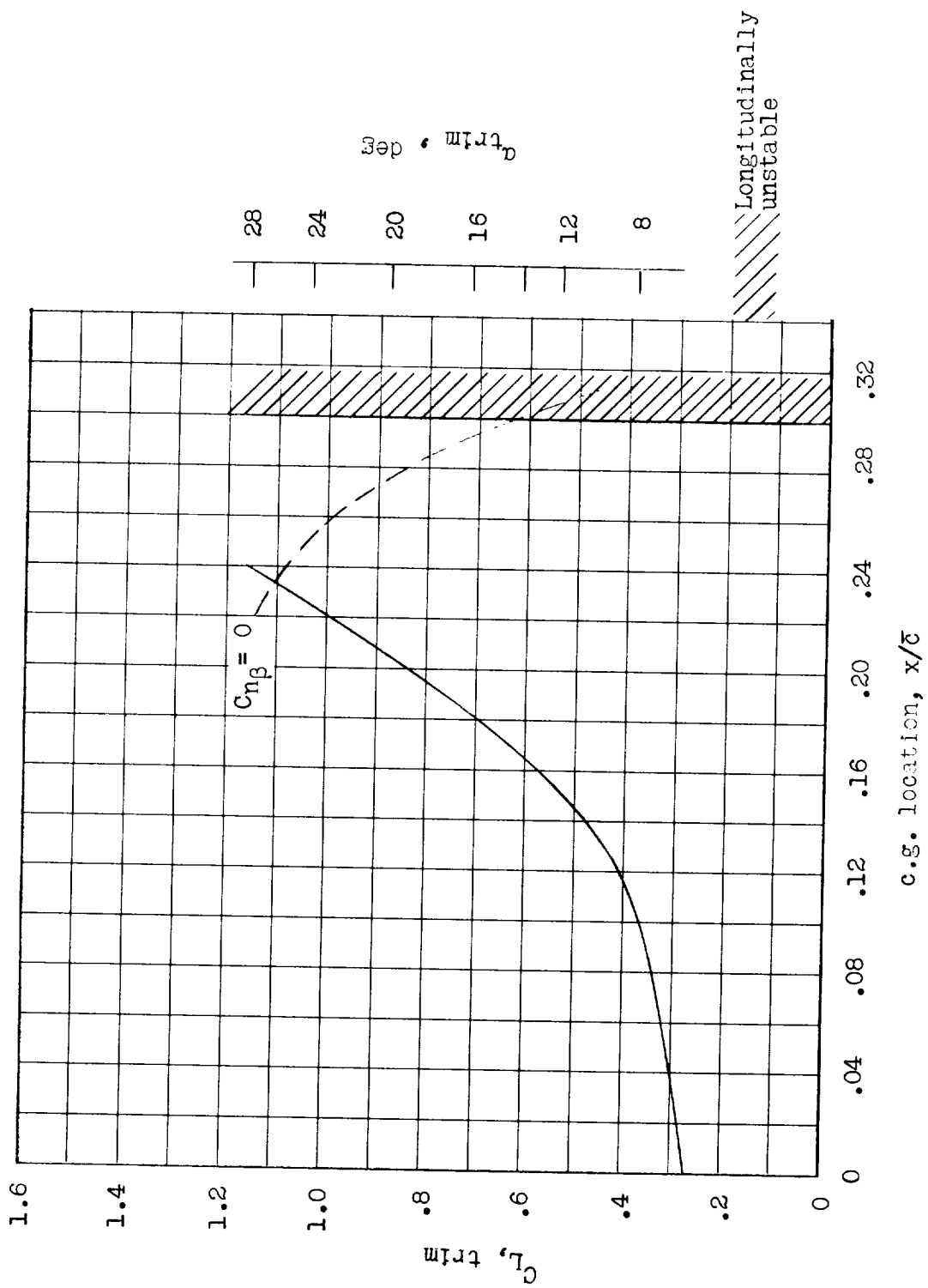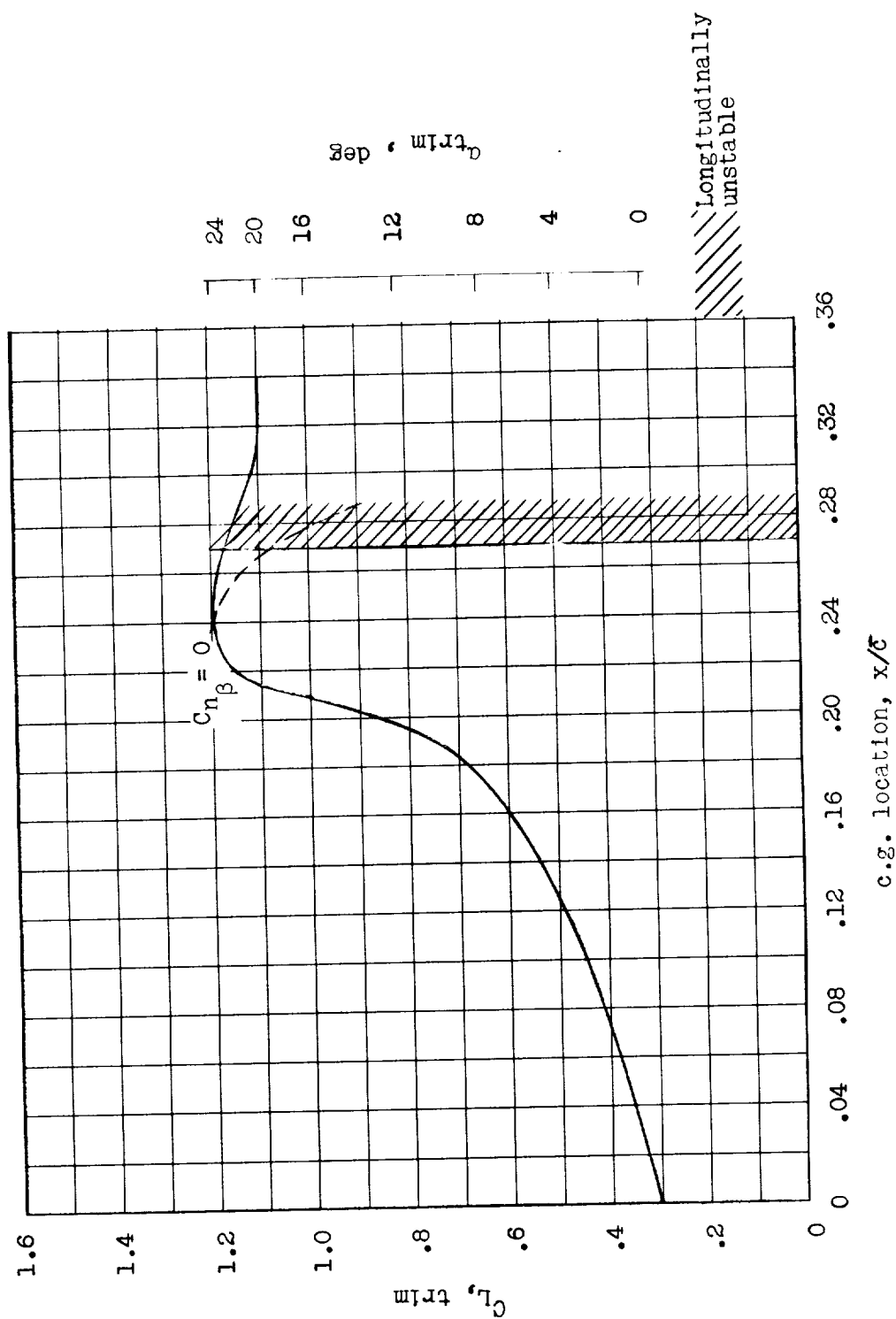
Figure 24.- Lateral characteristics of model II. $i_w = 0^o$; $\delta_f = 10^o$; high-lift canard, $C_{\mu,t} = 0$; center of gravity located at $0.275\bar{c}$.
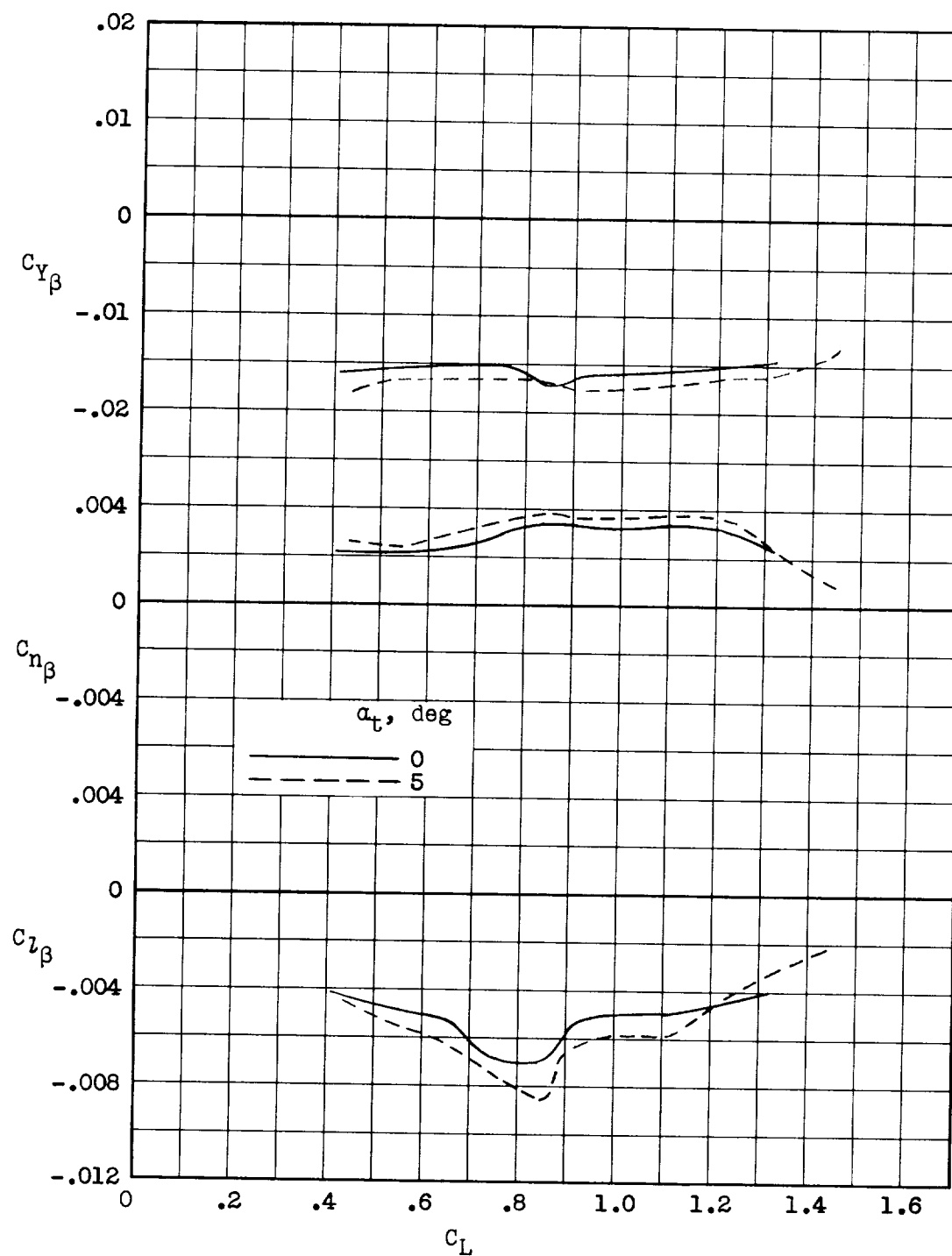
Figure 25.- Lateral characteristics of model II. $i_w = 12°$; $\delta_f = 10°$; high-lift canard, $C_{\mu,t} = 0.025$; center of gravity located at $0.275\bar{c}$.
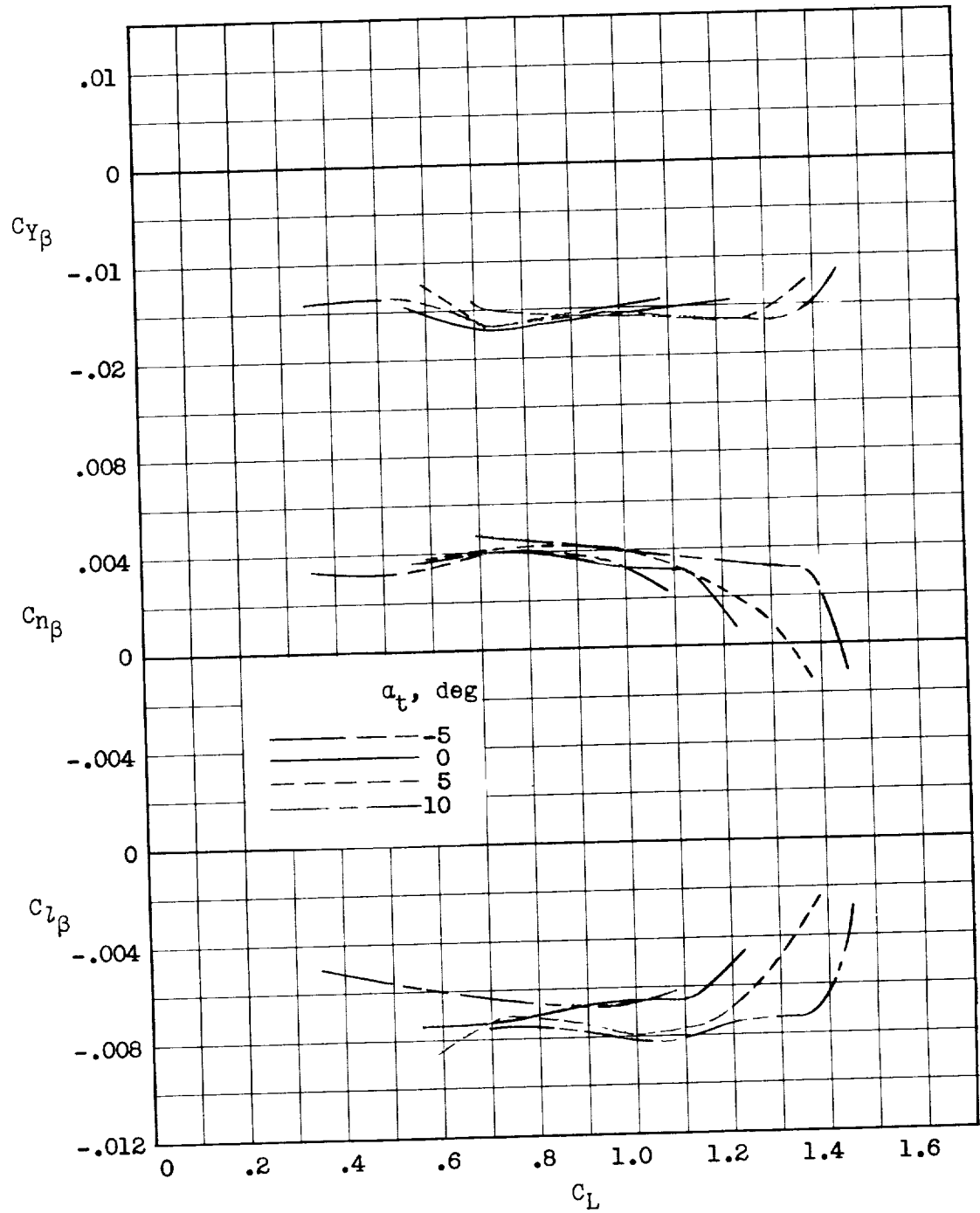
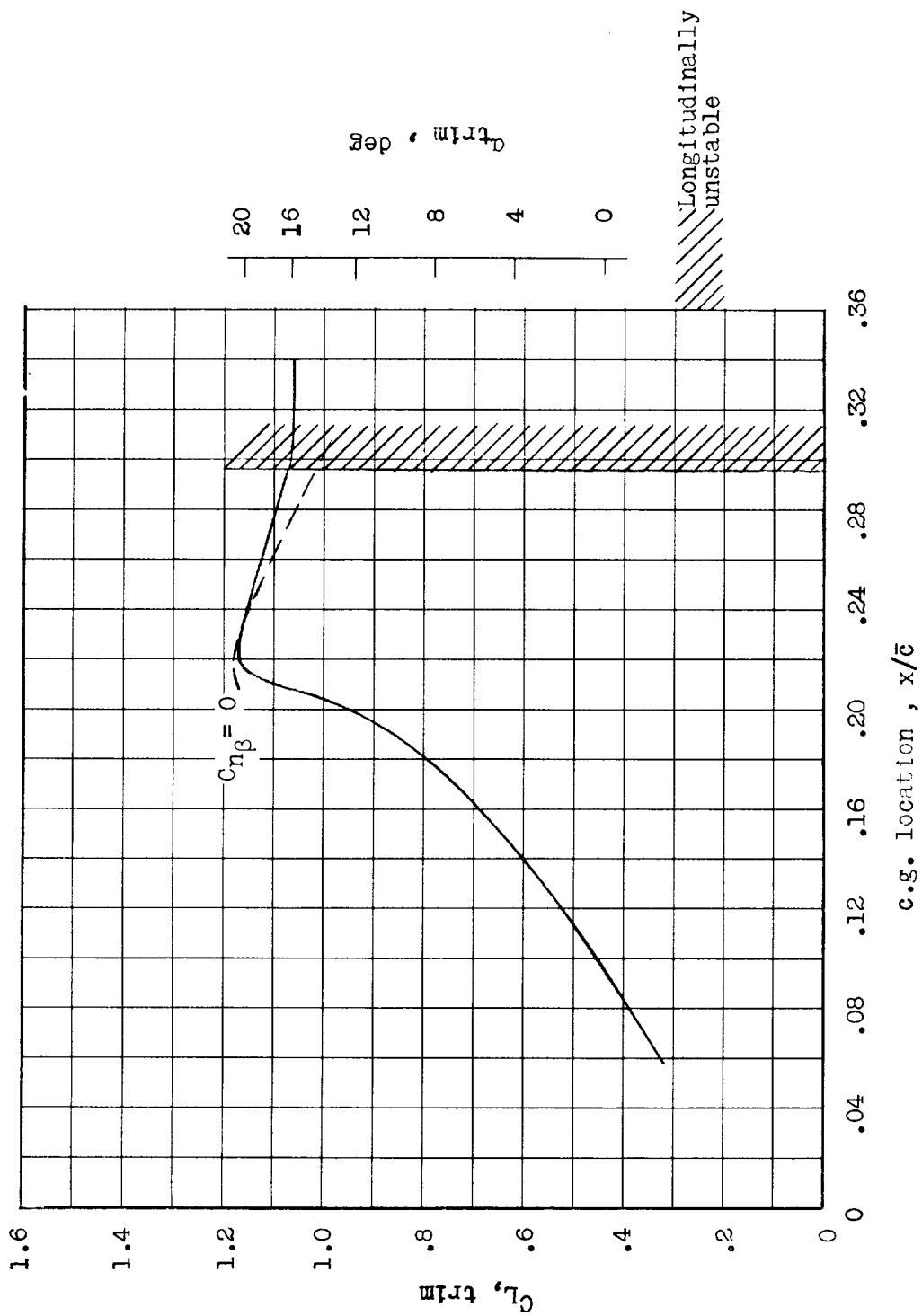Figure 26.- Lateral characteristics of model II. $i_w = 12^o$; $\delta_f = 10^o$; high-lift canard in high position, $C_{\mu,t} = 0.025$; center of gravity located at $0.275\bar{c}$.
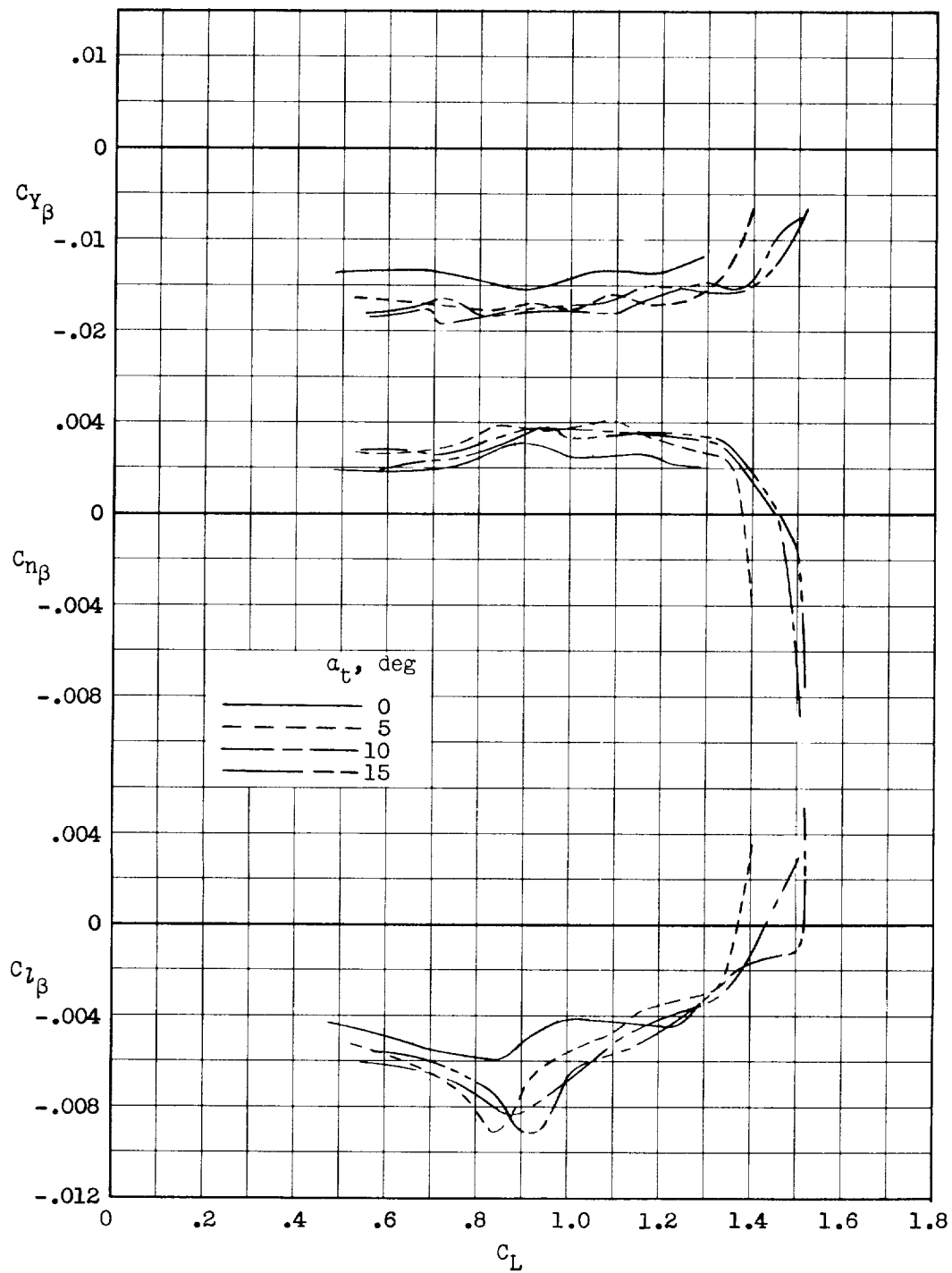
Figure 27.- Lateral characteristics of model II. $i_w = 12^\circ$; $\delta_f = 20^\circ$; high-lift canard, $C_{\mu,t} = 0$; center of gravity located at $0.275\bar{c}$.
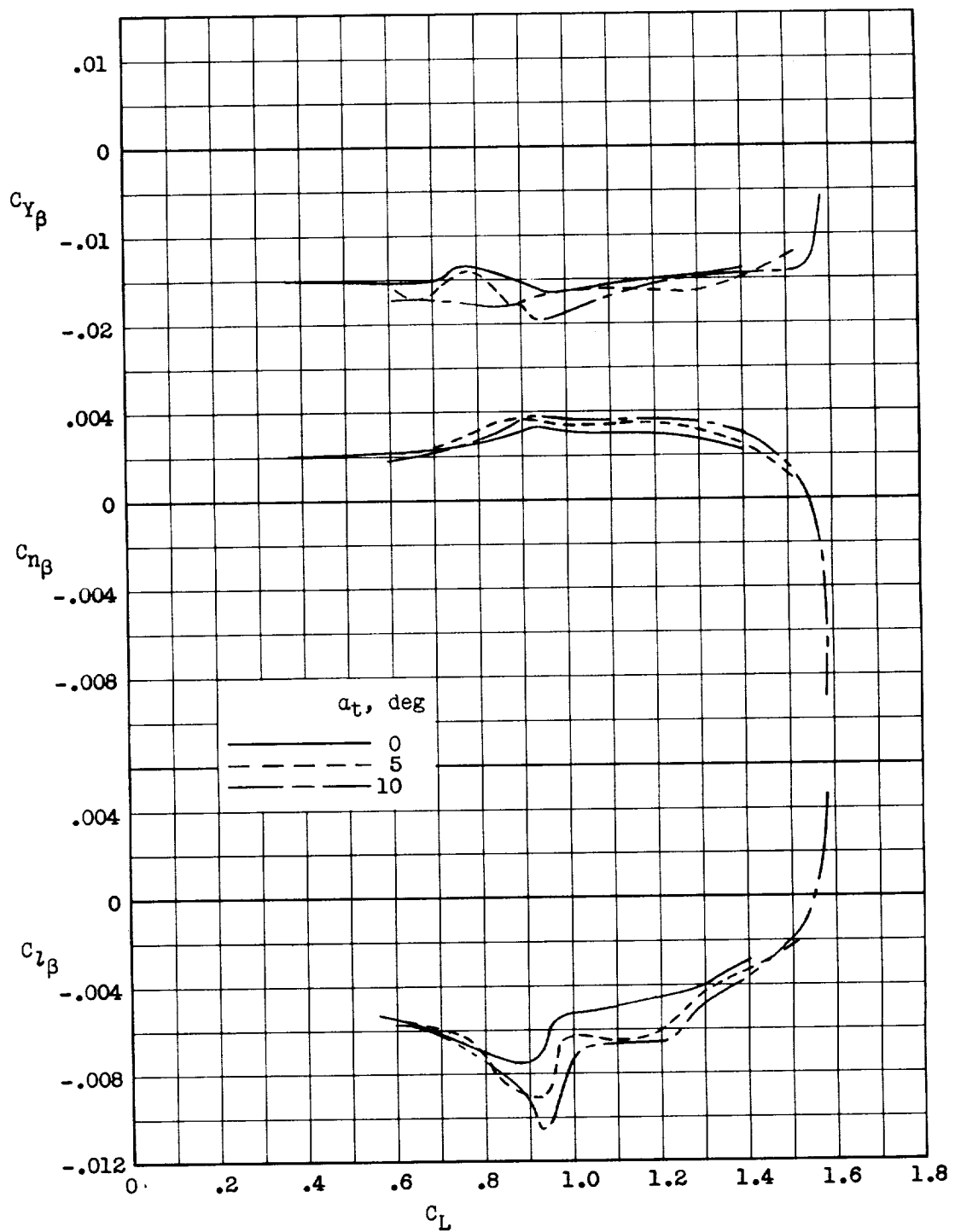
Figure 28.- Lateral characteristics of model II. $i_w = 12^o$; $\delta_f = 20^o$; high-lift canard, $C_{\mu,t} = 0.025$; center of gravity located at $0.275\bar{c}$.

(a) Basic model; $i_w = 0°$.

Figure 29.- Summary of static aerodynamic characteristics of model I.

56

(b) $i_w = 8°$.

Figure 29.- Continued.

(c) $i_w = 12^o$.

Figure 29.- Concluded.
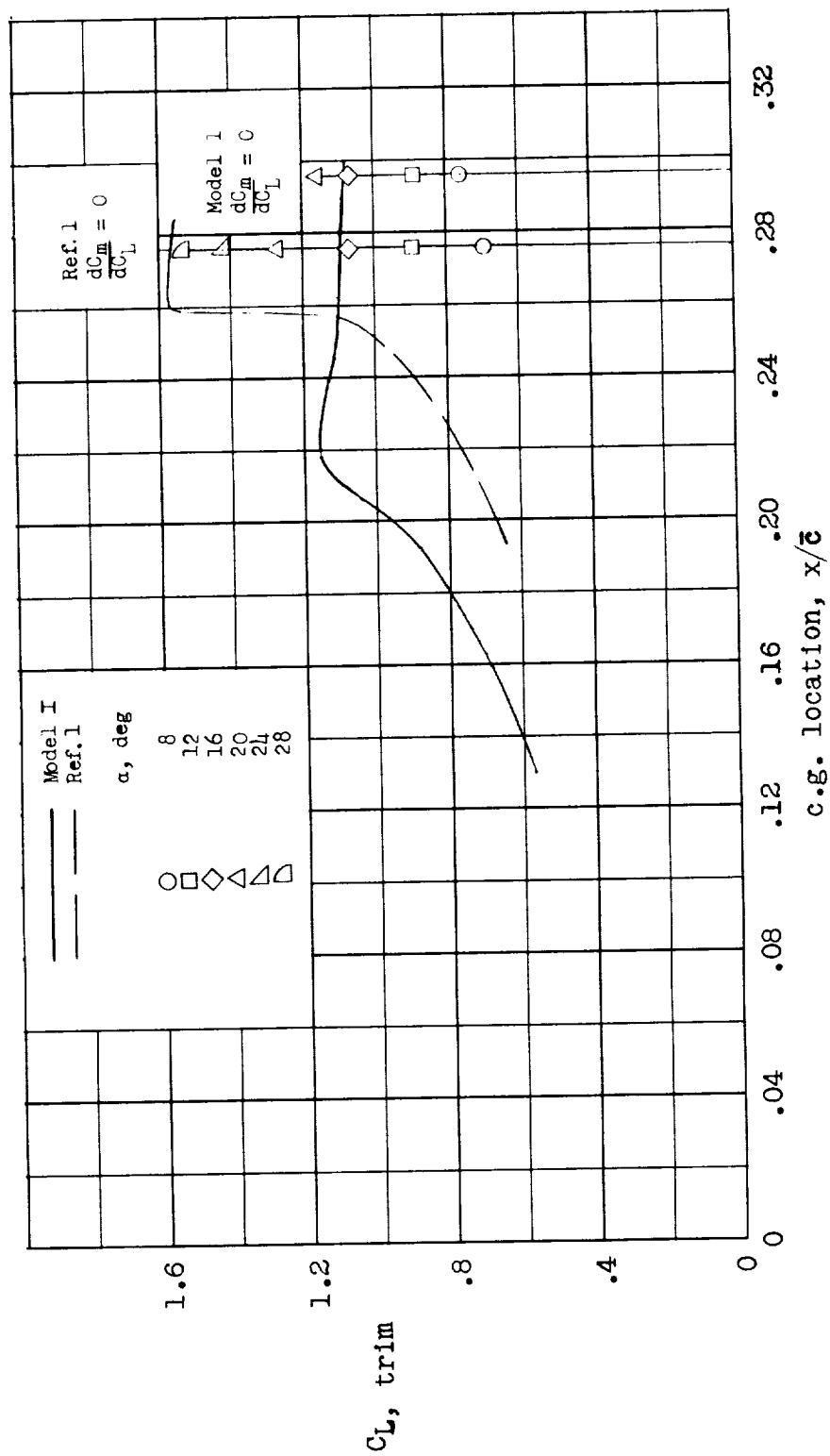
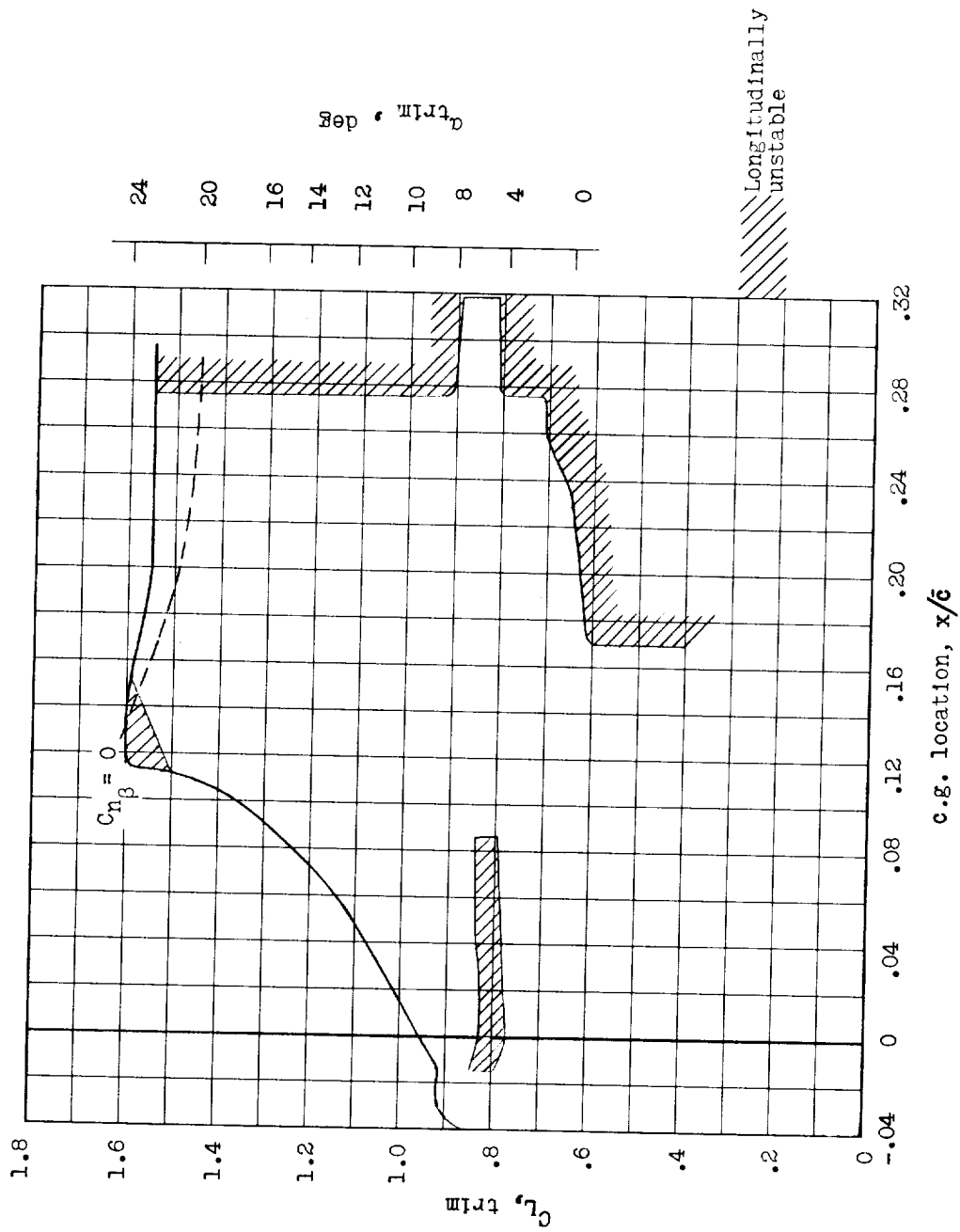Figure 30.- Comparison of the longitudinal trim characteristics of model I with those of the model of reference 1.
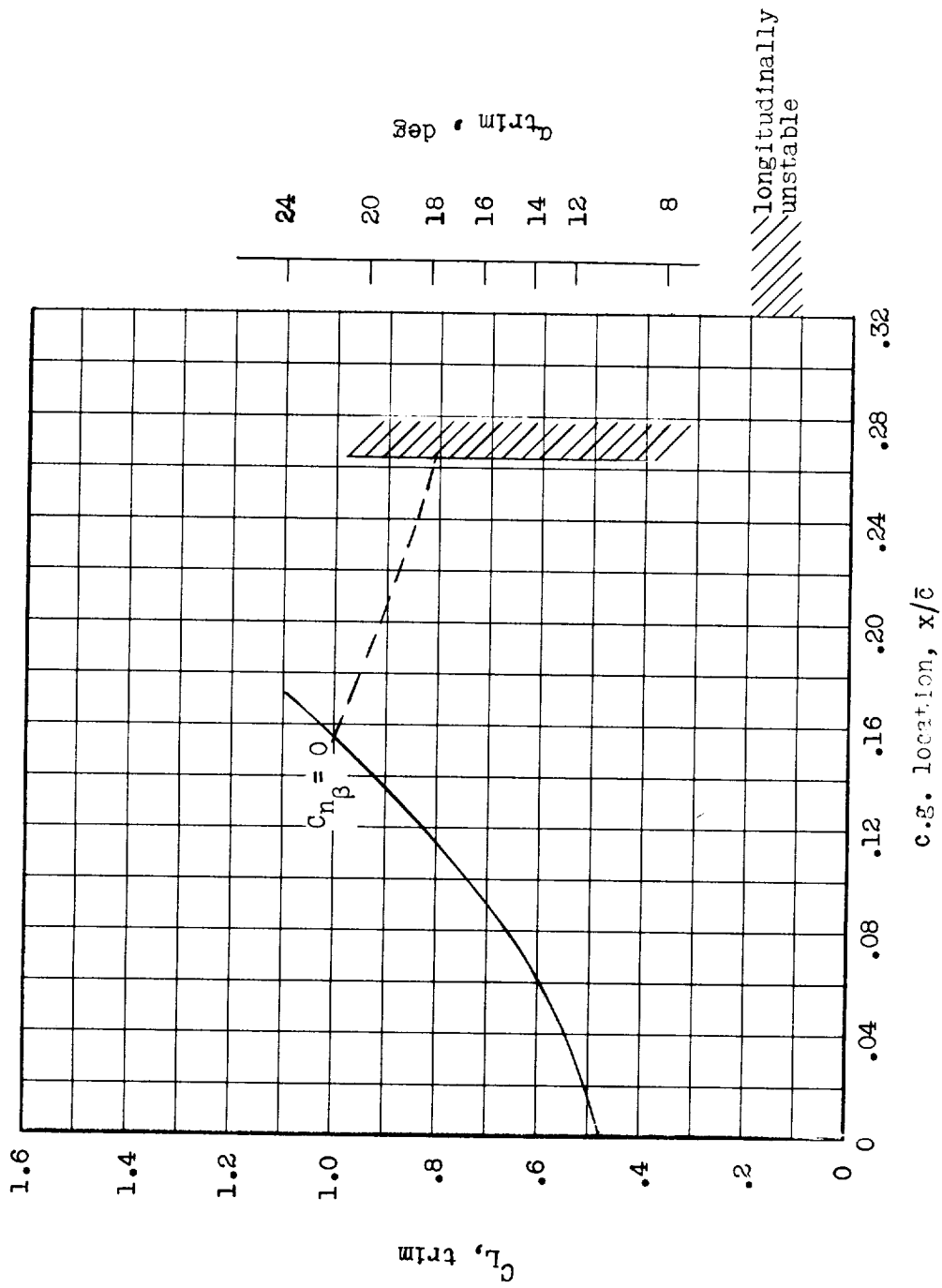
(a) Basic model; $i_w = 0°$.

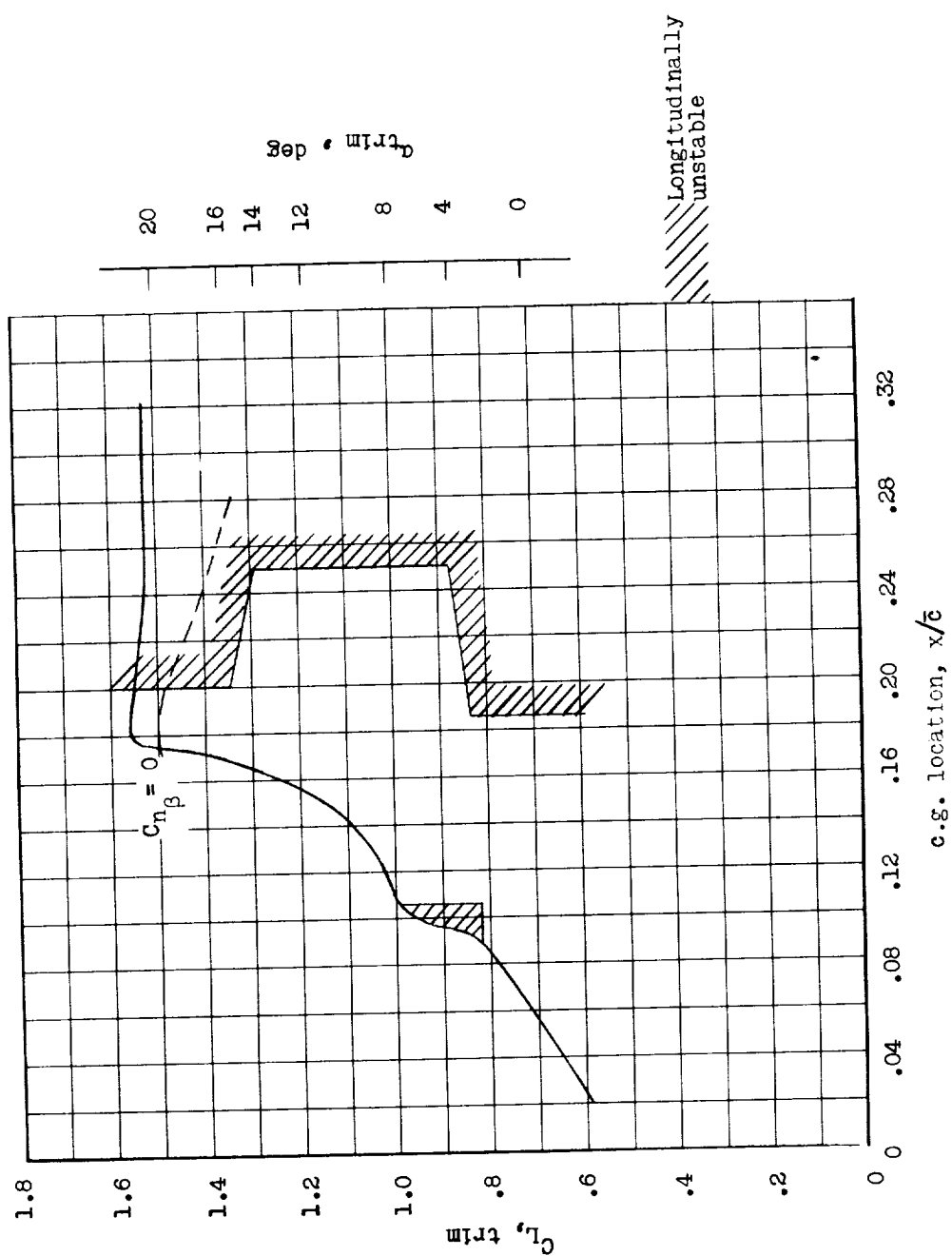Figure 31.- Summary of static aerodynamic characteristics of model II.

60
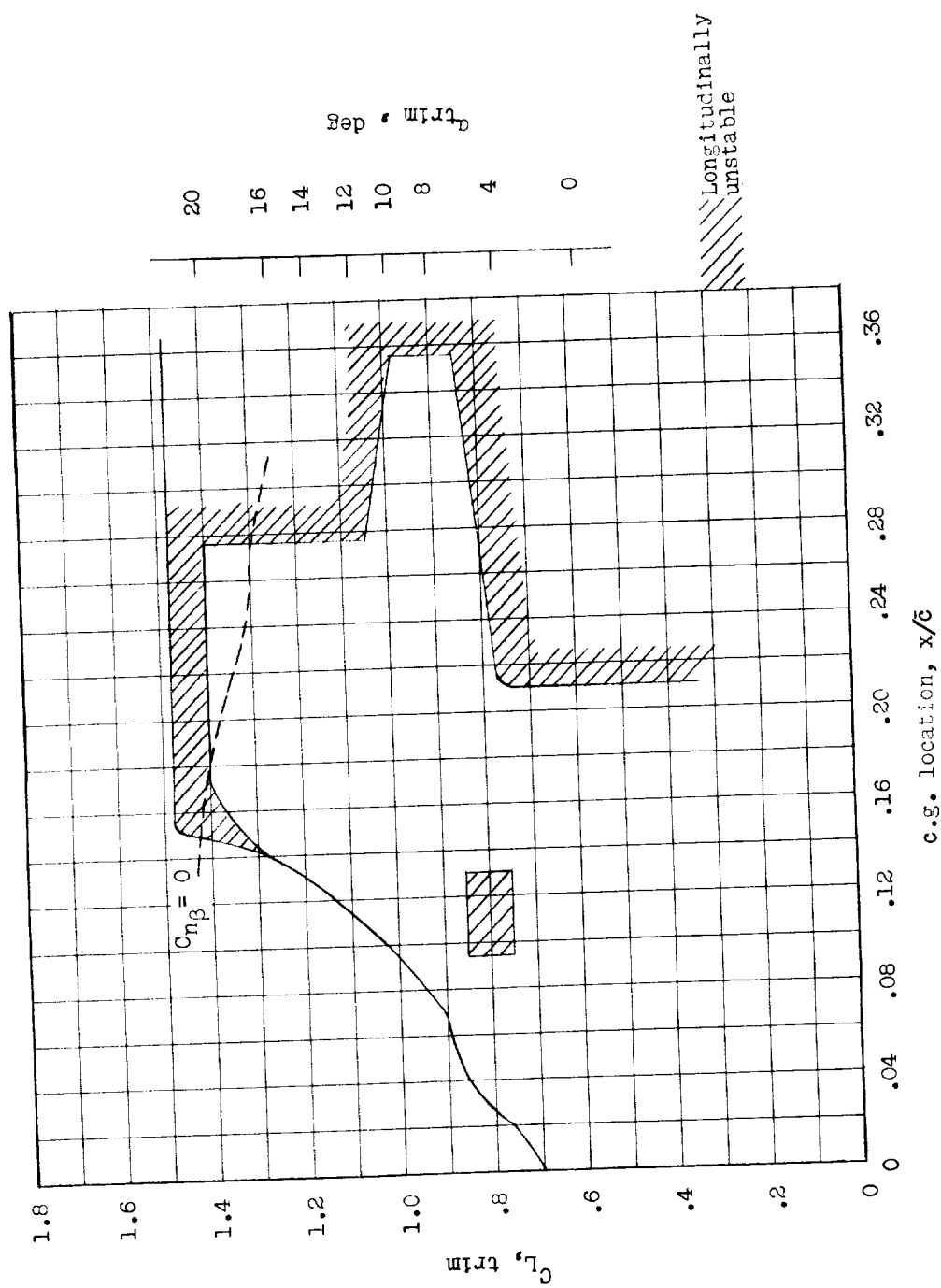
(b) $i_w = 12°$; $\delta_f = 10°$; $C_{\mu,t} = 0$.

Figure 31.- Continued.

(c) $i_w = 12°$; $\delta_f = 10°$; $C_{\mu,t} = 0.025$.

Figure 31.- Continued.

62

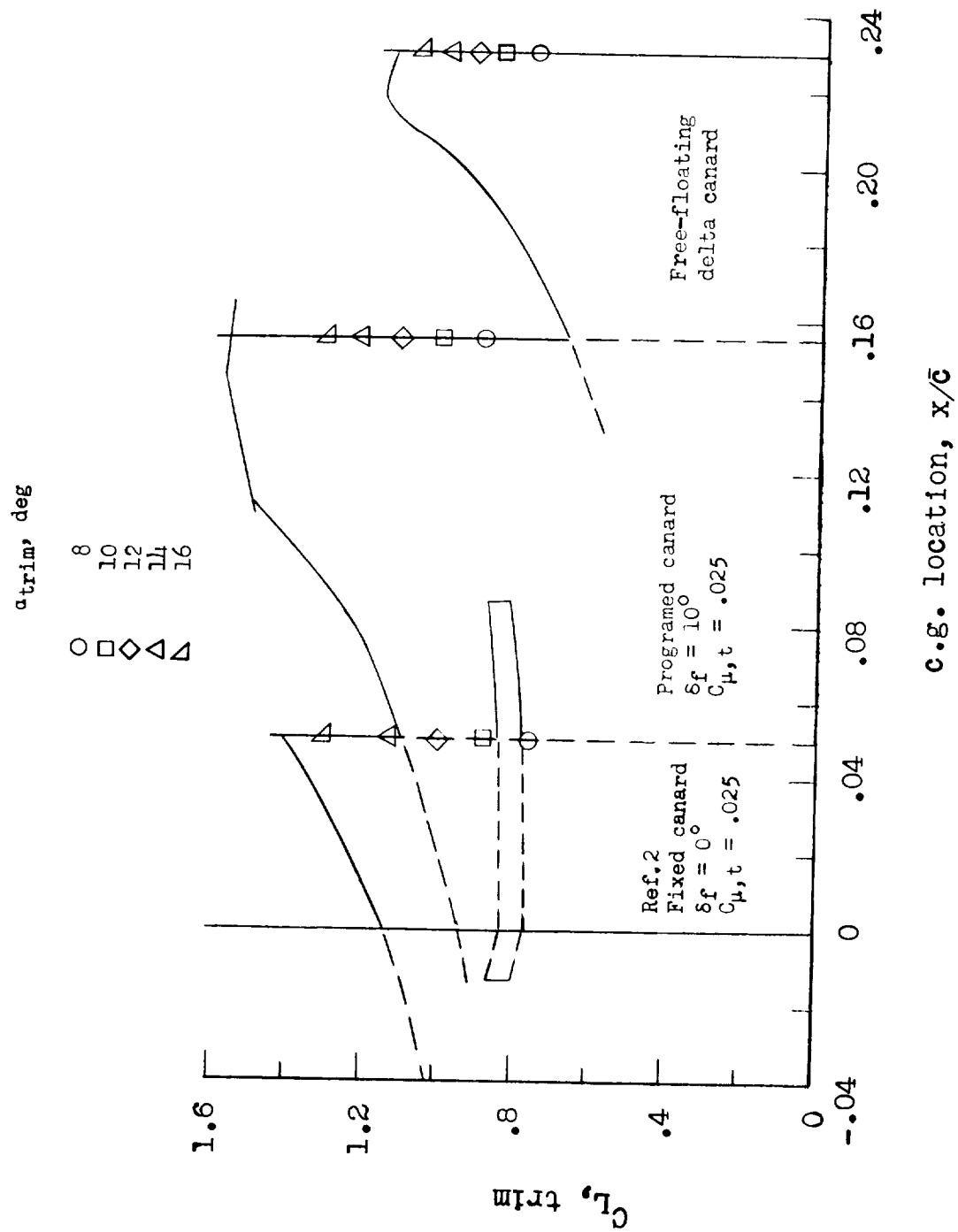(d) $i_w = 12^o$; $\delta_f = 20^o$; $C_{\mu, t} = 0$.

Figure 31.- Concluded.

Figure 32.- Comparison of the longitudinal trim characteristics of a fixed canard, a programed high-lift canard, and a free-floating canard.
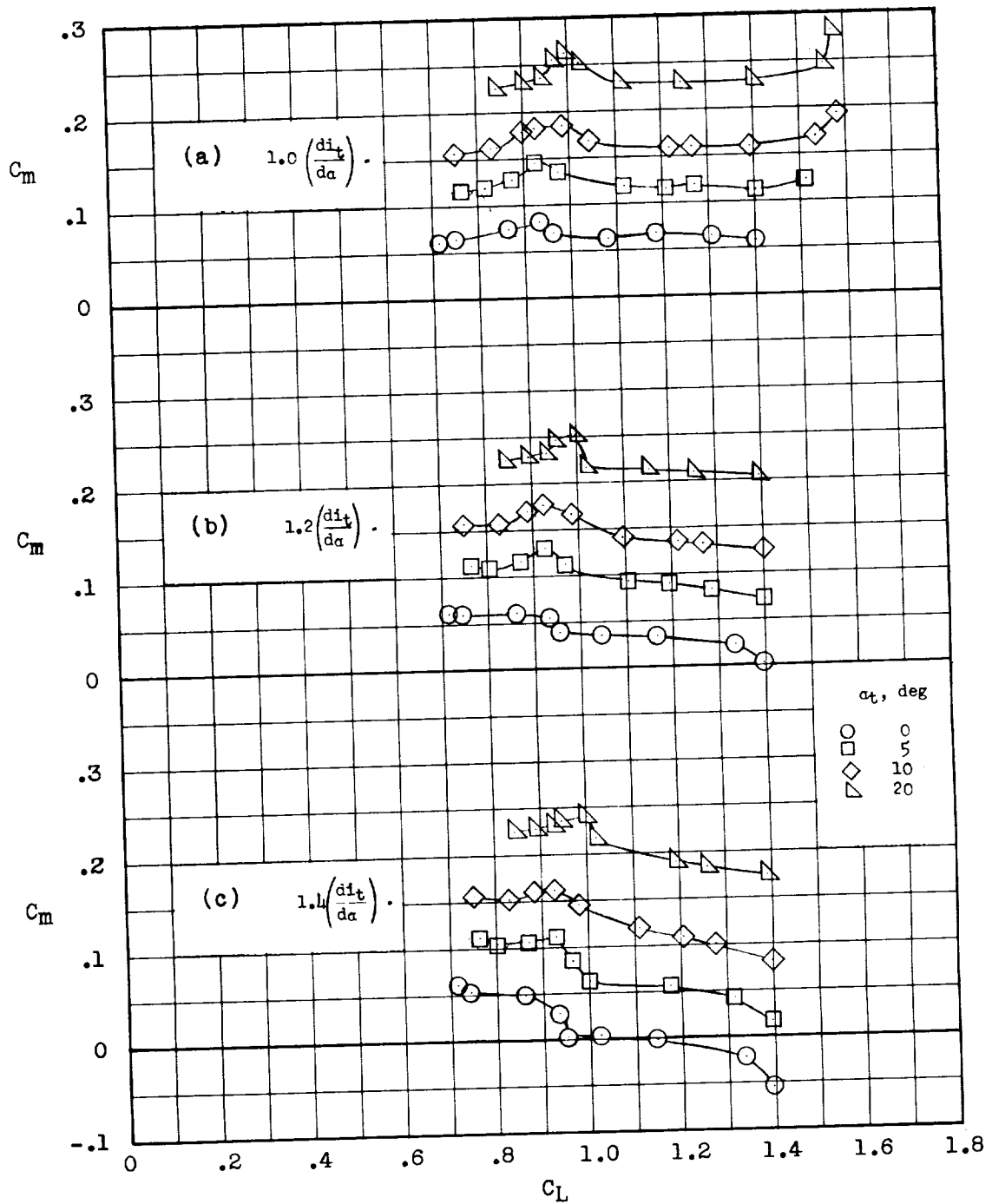
Figure 33.- Effect of increasing the rate of canard incidence with angle of attack $di_t/d\alpha$ on the static longitudinal stability of model II. $i_w = 12^\circ$; $\delta_f = 20^\circ$; $C_{\mu,t} = 0.025$; center of gravity located at $0.275\bar{c}$.